DUPLICATE

Numerical Weather Prediction

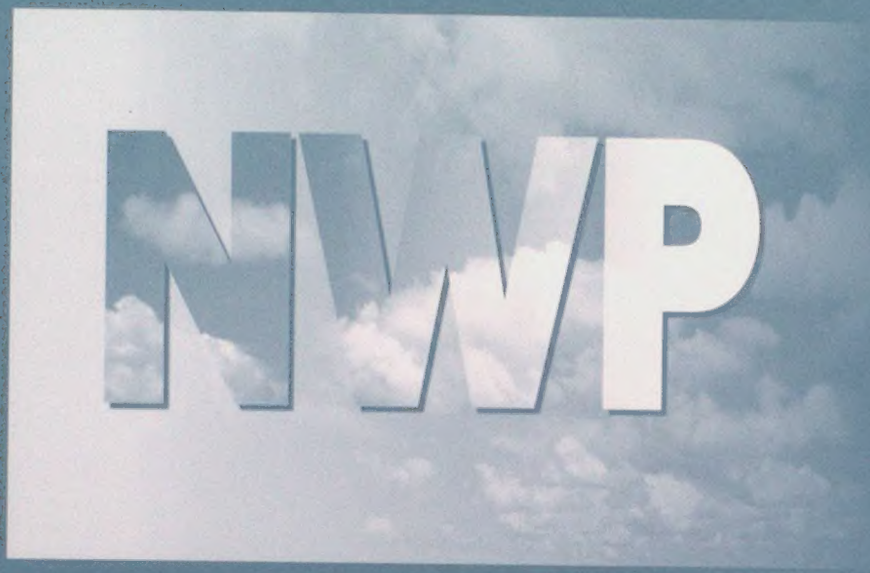

Forecasting Research Technical Report No. 371

An improved cloud detection scheme for Nimrod

By S. Watkin

October 2001

© Crown Copyright 2001

Met Office , Forecasting Development , Room R321, London Road , Bracknell , Berkshire ,RG12 2SZ, United Kingdom

Forecasting Research
Technical Report No. 371

An improved cloud detection scheme for Nimrod

by

S. Watkin

October 2001

The Met Office
NWP Division
Room 344
London Road
Bracknell
RG12 2SZ
United Kingdom

© Crown Copyright 2001

Permission to quote from this paper should be obtained from the above Met Office division

Please notify us if you change your address or no longer wish to receive these publications.

Tel: 44 (0)1344 856245 Fax: 44 (0)1344 854026 email: jsarmstrong@meto.gov.uk

An improved cloud detection scheme for Nimrod

Sarah Watkin

Satellite Imagery Applications Group
NWP Division
Met Office

October 2001

Abstract

A new cloud detection scheme has been developed for Nimrod which uses infrared and visible image data from Meteosat. The visible-based component has been operational since 1996 and remains unchanged, whilst the infrared-based component has been significantly upgraded. The new infrared-based scheme uses RTTOV, a radiative transfer model, to simulate the clear sky brightness temperature for each grid point using Mesoscale Model forecast data as inputs. These simulated brightness temperatures minus an offset, which is a function of surface type, are compared with the Meteosat infrared brightness temperature to determine whether a pixel is mainly clear or mainly cloudy. This scheme replaces the old infrared-based scheme that used the Mesoscale Model surface temperature minus an offset (ignoring effects of the gaseous atmosphere) as the threshold for each pixel. During the daytime, estimates of cloud cover from the infrared and visible-based components are combined to produce a cloud cover analysis. However, at night only the infrared-based scheme is used to generate a cloud cover analysis.

Validation tests involving statistical comparisons between the old and new infrared-based schemes and visual inspection of the cloud cover analyses show that the new infrared-based scheme produces a better overall representation of cloud cover than the old infrared-based scheme. In particular, the representation of cloud cover over the sea has significantly improved. Heidke skill score and equitable threat score have increased from 0.72 and 0.57 to 0.79 and 0.66, respectively, with the introduction of the new infrared-based scheme. Pre-operational tests demonstrated the robustness of the code and the performance during winter and summer months. In general, the operational implementation of the new infrared-based cloud detection scheme should result in more accurate cloud cover analyses during both day and night and a smoother transition between daytime (combined visible and infrared thresholding) and night-time (infrared thresholding) schemes at twilight.

Contents

Abstract 1

Contents 2

1. Introduction 3

1.1. Old cloud detection scheme 3
1.2. Motivation for the development of a new IR-based cloud detection scheme 3

2. Description of the new cloud detection scheme 4

2.1. Meteosat satellite data 4
2.2. New IR-based cloud detection scheme 5

3. Radiative transfer modelling 5

3.1. Description of RTTOV in Nimrod 5
3.2. RTTOV performance 7
3.2.1. Errors in mountainous areas 7
3.2.2. Effect of satellite viewing angle on clear sky BT 8
3.2.3. Comparison of clear sky BT with MES forecast surface temperature 9
3.2.4. Land - sea differences 10

4. Results of validation tests 11

4.1. Statistical performance of the new IR-based cloud detection scheme 11
4.2. Visual inspection 16
4.2.1. Selection of the optimum offsets: example on 28/02/2001 16
4.2.2. Sunrise on 16/10/2001 16
4.2.3. Comparison with NNCC at sunrise on 02/10/2001 17
4.2.4. Underestimation of cloud cover on 09/03/2001 17

5. Description of the code 23

5.1. Code structure and sequence of events 23
5.2. Run time and flexibility 24

6. Summary 25

References 26

Acronyms 27

Acknowledgements 27

Appendix 1: Graphs of the mean values of the statistical parameters for each month 28

Appendix 2: Structure of the operational cloud detection code on Nimrod 32

1. Introduction

Cloud cover analyses derived from Meteosat satellite imagery form an integral part of the Nimrod system. The main requirement for cloud cover analyses and forecasts comes from aviation, utilities, leisure industries and the general public, which require information about ground visibility and the impact of cloud on sunshine amounts (Golding, 1998). Further products, including cloud top height and multi-layer cloud analysis follow on from the cloud cover analysis on the Nimrod system.

The cloud detection scheme on Nimrod produces a cloud cover analysis from Meteosat imagery and Mesoscale Model (MES) forecast fields. The analysis shows the distribution of mainly cloudy and mainly clear pixels in the Nimrod domain. There are only two outcomes from the detection scheme: clear and cloudy, and therefore a pixel that contains partial cloud could potentially be classified as either.

This report describes the development and validation of a new infrared (IR)-based cloud detection scheme. In order to test and validate the scheme Meteosat imagery and MES forecast fields were archived on Nimrod during Winter 2000/01. Between 21/11/2000 and 31/03/2001 248 cases were archived (121 daytime, 127 night-time). The archived data included all the data needed to run the old scheme and the new scheme, so that comparisons could be made in validation tests. Real-time validation tests were also carried out.

1.1. Old cloud detection scheme

The old cloud detection scheme, in use from Spring 1996 until the completion of this work, consisted of two thresholding techniques: an IR-based cloud detection scheme and a visible-based cloud detection scheme. The Meteosat IR brightness temperature (BT) is compared to the MES surface temperature to determine whether a pixel is clear or cloudy (Golding, 1998). At night, or in daylight if a pixel is snow covered, a pixel is considered cloudy if the IR brightness temperature is at least 6.0 K colder than the model temperature. During the daytime the offset is increased to 7.5 K because cloud can also be identified using visible imagery. The normalised visible image is compared with a monthly cloud-cleared reflectance map obtained during 1995/96 (Jackson, 1995). A pixel is labelled cloudy if the normalised reflectance exceeds the clear sky value by 10 %; at noon this is increased to 15 %. In the daytime if either test detects cloud in a pixel then the pixel is labelled cloudy.

1.2. Motivation for the development of a new IR-based cloud detection scheme

Subjective investigation has shown that the old cloud detection scheme results in good discrimination between mainly clear and mainly cloudy pixels when both IR and visible images are available (Golding, 1998). However, it is recognised that the old scheme performs unsatisfactorily at night, when only IR imagery is available. It has been noted that the cloud cover analysis of areas of stratocumulus over the sea is particularly poor.

In 1997/98 experiments were conducted to assess the use of output from a fast radiative transfer model (RTM) in an IR thresholding technique for the cloud detection scheme on Nimrod (Whyte, 1998). The experiment used a RTM, called RTTOV, to simulate the IR BT expected from a clear atmosphere. By comparing the measured Meteosat IR BT against these simulated values, minus an offset, the atmospheric effect could be accounted for allowing more accurate estimates of cloud cover. Although the experimental scheme showed improvements over the old IR scheme (described

in Section 1.1) in some cases, the optimum offset varied from case to case. Therefore, the experimental scheme was not operationally implemented.

Problems noted in these experiments included: a bias in the RTTOV output, errors in MES surface temperatures and Meteosat calibration errors (Whyte, 1998). Since the experiments were conducted all of these problems have been addressed to some extent. The bias in the current RTTOV (RTTOV-6) clear sky calculations is known to be small, 0.1-0.2 K, so it is not thought that this should pose a problem for cloud detection (Saunders, pers. comm.). AVHRR-retrieved sea surface temperatures are now assimilated into the MES, so the MES surface temperature field has been improved. Also, a new calibration scheme was introduced on 29/05/2000 for Meteosat –7 using a blackbody calibration method that corrected a bias of 0.8 % in the IR radiances.

All of the factors noted in this section contributed to the decision that a new IR-based cloud detection scheme that uses RTTOV simulated clear sky radiances should be developed and tested. An additional impetus was the delay in the launch of the first Meteosat Second Generation (MSG) satellite. The current planning date for the launch is in mid 2002 (EUMETSAT web site). Cloud products generated from MSG data are planned to supersede cloud products generated from Meteosat data currently on Nimrod.

2. Description of the new cloud detection scheme

The new cloud detection system also consists of two thresholding techniques: a new IR-based cloud detection scheme and a visible-based cloud detection scheme. The visible-based cloud detection scheme has remained unchanged through the course of this project (see Section 1.1). A full description is presented by Jackson (1995).

2.1. Meteosat satellite data

IR and visible Meteosat data are the basis of the cloud detection scheme on Nimrod. The imager on Meteosat measures visible and IR radiances every half hour, in the spectral ranges of 0.45 - 1.0 and 10.5 - 12.5 μm respectively.

Meteosat satellite data are received at the Met Office every half hour and are processed on the Autosat system before the data are received on Nimrod. Autosat calibrates the IR Meteosat data using coefficients provided by EUMETSAT to convert the data from counts to radiances. These are then converted to BTs using a pre-calculated look-up table. BTs in the range 193.0 K to 303.0 K are set to values between 0 and 255. Thus, a range of 110 K is represented by 256 values resulting in a discretisation of IR BTs of 0.4 K. Visible Meteosat data remain uncalibrated and are simply represented by values in the range 0 to 255. Invalid satellite data are not represented by a specific value but are set to 255, therefore invalid data cannot subsequently be distinguished. Geolocated IR and visible data in the range of 0 to 255 are sent to Nimrod where further processing takes place.

Once on Nimrod the first stage is to re-map the data onto the National Grid in the Nimrod domain. This results in 345 x 435 pixels with a spacing of 5 km. The IR data are converted back to BTs in the range 193.0 K to 303.0 K. A normalisation factor is applied to the visible data that accounts for the solar zenith angle and scales the resulting values to represent albedos in the range 0.0 % to 100.0%. These data are then used in the operational cloud detection scheme.

2.2. New IR-based cloud detection scheme

The IR radiation measured by a satellite in clear sky originates from the surface of the earth and from the intervening atmosphere. In order to detect the presence of cloud, the radiative signal in clear sky conditions must first be determined. The old IR-based scheme made the approximation that the MES surface temperature minus an offset represented the clear sky IR BT. The surface radiation is by far the largest component of the top of the atmosphere radiance in the IR window, but it does not take account of the absorption and emission of radiation by the atmosphere. To take account of these radiative interactions a RTM is employed to simulate the clear sky radiance as measured by Meteosat. The radiative transfer model, RTTOV, is described in Section 3.

MES forecast data are used as inputs to RTTOV. Every hour RTTOV is run to simulate the clear sky BTs for each Nimrod grid point on a 15 km National Grid. Every half hour Meteosat BTs on a 5 km National Grid are compared with the simulated clear sky BT to determine whether a pixel is clear or cloudy. For each Meteosat grid point, the nearest model grid point is found and used in the comparison. If the Meteosat IR BT is less than the simulated clear sky BT minus an offset, then the grid point is labelled as cloudy. The offset was determined from the validation tests described in Section 4.

New IR-based cloud detection scheme:

Meteosat IR BT < Simulated clear sky BT - offset $\Longrightarrow$ cloudy

Meteosat IR BT ≥ Simulated clear sky BT - offset $\Longrightarrow$ clear

3. Radiative transfer modelling

The radiative transfer model implemented in the new IR-based cloud detection scheme is RTTOV-6 (Eyre, 1991; Saunders, 2000). RTTOV is a fast radiative transfer model that simulates the top of the atmosphere radiance for a specific satellite instrument over a specified surface type (sea, land or snow/ice). It uses inputs of temperature, specific humidity and ozone amount on 43 pressure levels and surface inputs of temperature, specific humidity, pressure and u and v wind speeds.

3.1. Description of RTTOV in Nimrod

MES forecast fields are used as inputs to RTTOV (Table 1). Each hour the forecast data valid for that hour with the shortest forecast lead time are determined. The 3D relative humidity (*RH*) data are converted to 3D specific humidity (*SH*) data using Tetens formula:

$$e_s = \exp\left(19.079 - \frac{4098.026}{T - 35.86}\right), \qquad (1)$$

$$SHMR = \frac{\varepsilon e_s}{p - e_s}, \qquad (2)$$

$$SH = RH x SHMR. \qquad (3)$$

Here, e_s is the saturated vapour pressure, T is the temperature in Kelvin, *SHMR* is the saturated humidity mixing ratio in kg/kg, ε is the ratio of the gas constant of dry air to the gas constant of water vapour (approximately, $\varepsilon = 0.62$) and p is the air pressure. The MES 3D temperature and pressure fields are used to compute the saturated humidity mixing ratio using Equations 1 and 2. The specific humidity is then computed using Equation 3.

Input to RTTOV	Data used on Nimrod	Units
Temperature profile on 43 levels	MES forecast 3D temperature *datetime//'_nimrod_ng_umfc_3dtemperatureFCST_15km*	K
Specific humidity profile on 43 levels	MES forecast 3D relative humidity *datetime//'_nimrod_ng_umfc_3drelhumidityFCST_15km*	kg/kg
Ozone profile	Reference profile on 43 levels (provided with RTTOV code)	kg/kg
Surface 2m temperature	Lowest model level from MES forecast 3D temperature *datetime//'_nimrod_ng_umfc_3dtemperatureFCST_15km*	K
Surface 2m specific humidity	Lowest model level from MES forecast 3D relative humidity *datetime//'_nimrod_ng_umfc_3drelhumidityFCST_15km*	kg/kg
Surface pressure	Lowest model level from MES forecast 3D pressure *datetime//'_nimrod_ng_umfc_3dpressureFCST_15km*	hPa
Radiative skin temperature	MES forecast surface temperature *datetime//'_nimrod_ng_umfc_surftempFCST_15km*	K
Surface type	Land = 0, sea = 1, snow/ice = 2 determined for each gridpoint using: *constant_nimrod_ng_nimrod_orography_15km* *cdatetime//'_nimrod_ng_umfc_snowdepthFCST_15km*	none
Meteosat zenith angle	Calculated for each grid point in the Nimrod domain	degrees

Table 1. RTTOV inputs. Where Nimrod data have been used the filename is shown in italics. Here, datetime is the date and time in the form YYYYMMDDHHMM, and FCST is the forecast lead time in minutes. Meteosat zenith angles are calculated for each grid point using a series of calculations that translates grid point position to Meteosat zenith angle at the earth's surface. Wind speeds, u and v, are set to zero.

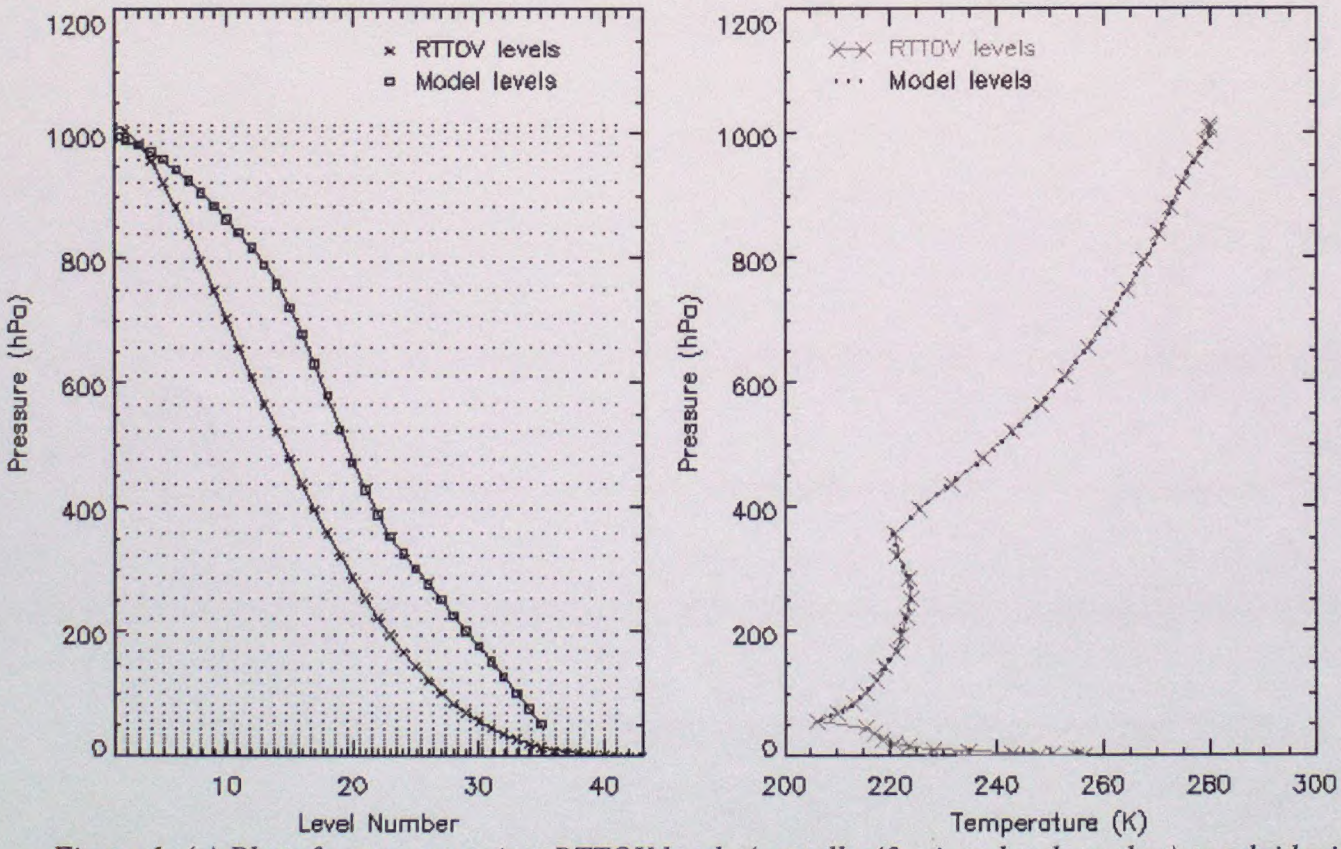

Figure 1. (a) Plot of pressure against RTTOV levels (actually 43 minus level number) overlaid with an example of the pressure profile of the MES levels for one grid point at a single time. The MES currently has 35 moist levels on hybrid eta coordinates. (b) Plot of a MES forecast temperature profile (black dots) for 1200 UTC on 22/11/2001 overlaid with the same profile once it has been mapped onto RTTOV pressure levels (grey crosses).

The MES 3D temperature and 3D specific humidity fields are mapped from model levels to RTTOV pressure levels using the MES 3D pressure field. Figure 1(a) shows an example of the different levels used in the MES and RTTOV. The mapping routine linearly interpolates temperature and specific humidity data on a linear pressure scale. At the highest pressure levels in the RTTOV profile (i.e. near the surface) the levels are filled with the value of the lowest model level. RTTOV does not use data on pressure levels above the surface pressure, thus the data values in the highest RTTOV pressure levels are arbitrary. In the lowest pressure RTTOV levels (i.e. at the top of the atmosphere), above the top of the MES model levels, the RTTOV reference profile is used. Again, the data values used at the top of the profile are arbitrary because RTTOV is being used to simulate the BT in a window channel (10.5 - 12.5 μm) and thus the meteorological characteristics of the upper atmospheric levels have little effect on the resultant BT. Figure 1(b) demonstrates the high accuracy of the mapping routine and shows a pre-mapped MES forecast 3D temperature profile (black dots) and a post-mapped temperature profile on RTTOV levels (grey crosses).

A RTTOV BT simulation is performed for each grid point in the Nimrod domain at a spacing of 15 km (i.e. 115 x 145 grid points). A Nimrod format file containing these BTs (10 x deg K) is written every hour.

The RTTOV computations performed here are specific to Meteosat-7. RTTOV-6 is set up to simulate BT for the IR channels on the Spinning Enhanced Visible and Infrared Imager (SEVIRI), the imager on Meteosat Second Generation (MSG). Therefore, the cloud detection scheme presented here could be adapted to operate using 10.8 μm BT data from SEVIRI.

3.2. RTTOV performance

3.2.1. Errors in mountainous areas

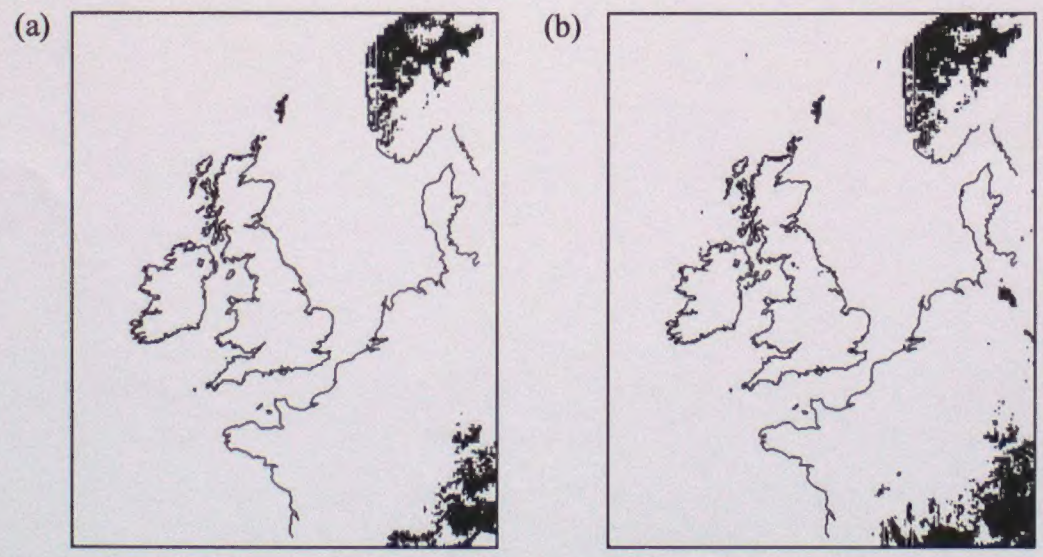

Figure 2. Map of the Nimrod domain showing grid points where (a) Meteosat IR BT is greater than the MES surface temperature by 0.4 K or greater (5% of grid points), and (b) Meteosat IR BT is greater than the simulated clear sky BT by 0.4 K or greater (10% of grid points), in any of the eight cases considered (between 21/11/2000 and 11/02/2001). A threshold of 0.4 K was chosen because the discretisation of Meteosat IR BT is 0.4 K.

In most situations, the MES surface temperature is greater than the simulated clear sky BT and Meteosat IR BT because the atmosphere absorbs a fraction of the IR radiation emanating from the earth's surface and emits radiation from the atmosphere at a lower temperature than the earth's surface. A meteorological condition that can cause the Meteosat IR BT to be greater than the actual surface temperature is when there is a low level temperature inversion with low water vapour content in the atmosphere above.

Out of eight cases studied throughout the period of 21/11/00 to 11/02/01, all contained some grid points where the Meteosat IR BT is greater than the MES surface temperature and the simulated clear sky BT (Figure 2). The large majority of the grid points highlighted in Figure 2 are in mountainous regions. The cause of these anomalies is not thought to be due to any meteorological condition but due to errors in the MES surface temperature field. Due to the mismatch between the altitude of meteorological stations and MES orographic height in mountainous areas, observations from these stations are not assimilated (Macpherson, pers. comm.). Thus, errors in MES forecast surface temperature frequently occur in areas of high orography or steep gradients. Moreover, the MES forecast snow cover is known not to be very accurate, leading to misclassification of surface type for the RTTOV calculations. MES forecast surface temperature errors and surface type misclassification will lead to errors in the simulated clear sky BT. This is not a problem that can be solved for the Nimrod cloud detection scheme, but one that should be taken into account if the cloud detection scheme performs poorly in these regions. However, in pre-operational tests these errors have not caused a noticeable problem in the differentiation between clear and cloudy pixels.

3.2.2. Effect of satellite zenith angle on clear sky BT

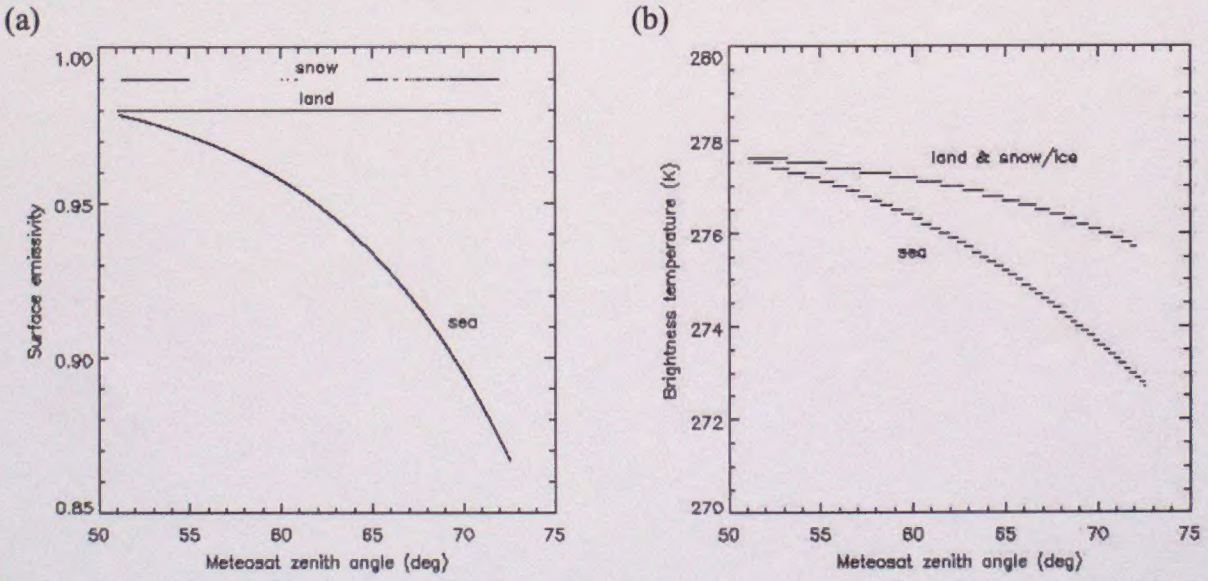

Figure 3. (a) Plot of surface emissivity, calculated by ISEM-6 in RTTOV, against Meteosat zenith angle for different surface types. (b) Graph of simulated clear sky BT against Meteosat zenith angle. The clear sky BT were simulated using profile and surface MES fields from a single grid point, but for the full range of Meteosat zenith angles in the Nimrod domain.

The simulated clear sky BT for a grid point depends not only on the meteorological characteristics of the atmosphere and the surface, but also on the satellite zenith angle for that grid point and the surface type. These two parameters determine the surface emissivity used in the RTTOV simulation. In ISEM-6, the Infrared Surface Emissivity Model for RTTOV-6, default emissivity models are implemented for different surface types (Table 2).

Surface type	RTTOV code	Default value
Land	0	0.98
Sea	1	Function of wavenumber and zenith angle*
Snow/ice	2	0.99

*Table 2. Surface emissivity values used in RTTOV-6 (Sherlock, 1999). *Emissivity is also a function of wind speed, but this is assumed to be zero in ISEM-6.*

The magnitude of the satellite zenith angle affects the simulated clear sky BT in two ways. As the zenith angle increases so the optical path length between the earth's surface and Meteosat increases, resulting in greater atmospheric absorption and lower BT. The second factor is the effect that zenith angle has on the modelled emissivity over the sea (Figure 3(a)). As zenith angle increases so sea surface emissivity decreases for a fixed wavelength. Figure 3(b) shows the effect of varying Meteosat zenith angle on the simulated clear sky BT. The meteorological inputs are constant for all grid points, thus the only parameters varying between grid points are the zenith angle and the surface type. In the profile used to generate the graph in Figure 3(b), an increase in zenith angle from 51.35° to 72.57° leads to a decrease in simulated clear sky BT of 2 K over land and snow/ice surfaces and 4 K over the sea. Therefore, use of the correct zenith angles in the RTTOV simulations is essential for accurate cloud detection.

3.2.3. Comparison of clear sky BT with MES forecast surface temperature

Comparisons were made between the simulated clear sky BT and MES forecast surface temperature to determine the range of atmospheric deficit values. The atmospheric deficit is the difference between the surface temperature and the top of the atmosphere BT, i.e. the reduction in temperature due to the presence of the atmosphere. The mean atmospheric deficit for 248 cases, between 21/11/2000 and 31/03/2001, each containing 115x145 grid points was 4.6 K. The maximum value was found to be 10.8 K, whilst the minimum value was -1.85 K. These values are consistent with typical atmospheric deficit values. Merchant et al. (1999) suggest that in atmospheric window regions, the brightness temperature of the radiation reaching the satellite sensor is typically lower by 1 to 10 K than would be the case were the atmosphere completely transparent and the surface black.

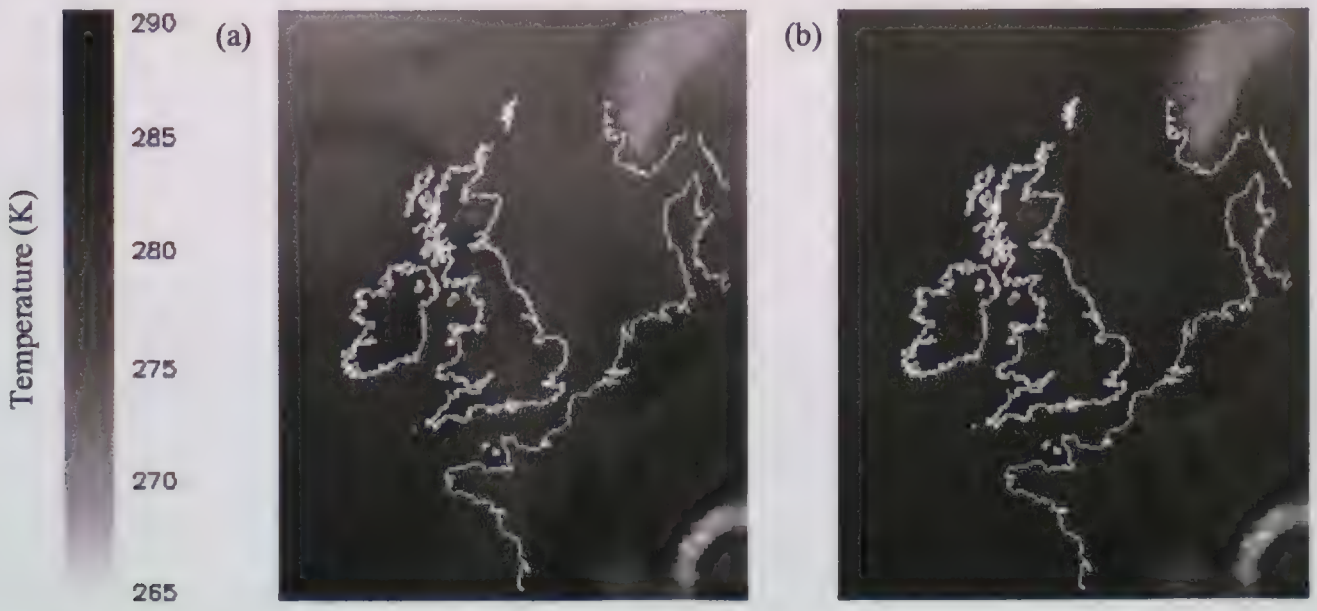

Figure 4. (a) Simulated clear sky BT and (b) MES forecast surface temperature on 05/12/2000 at 1300 UTC. The key for both images is on the left.

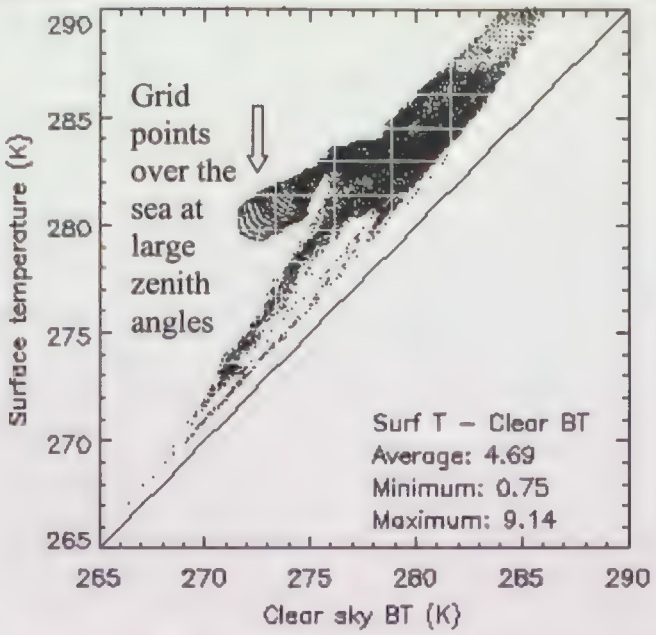

Figure 5. Graph of MES surface temperature against simulated clear sky BT for 05/12/2000 at 1300 UTC (same data as in Figure 4). The 1:1 line is also plotted.

Figures 4 and 5 show the simulated clear sky BT and the MES forecast surface temperature for a single case. The range of atmospheric deficit values is typical for the data collected. There are a couple of interesting features to point out. The major surface temperature patterns, e.g. low surface temperatures over the Alps and warm temperatures over The Netherlands are reproduced in the simulated clear sky BT. This demonstrates the significant influence that surface temperature has on the simulated clear sky BT, and therefore errors in MES forecast surface temperature will propagate to errors in simulated clear sky BT. Over the sea the simulated clear sky BT tends to decrease with increasing latitude due to the effect of Meteosat zenith angle on emissivity and path length, as discussed in Section 3.2.2. By comparison the sea surface temperature is approximately constant over the Nimrod domain again showing the strong effect of Meteosat zenith angle on the simulated clear sky BT. It is these grid points that have the largest atmospheric deficit values (Figure 5).

3.2.4. Land - sea differences

The Nimrod orography ancillary file on a 15 km National Grid is used to determine whether a grid point is on land or sea. Where the orography is at 0 km altitude the surface is assumed to be sea. Once the RTTOV simulations have been performed on the 15 km grid, the clear sky BT are used to set the variable threshold for each grid point on a 5 km grid so that a comparison can be made with Meteosat IR BT. For each grid point in the 5 km grid the nearest grid point in the 15 km grid is determined. Therefore, in coastal areas it is possible to be comparing a Meteosat IR BT over the land with a simulated BT over the sea, or vice versa. This has the potential to introduce small errors, particularly at large zenith angles, and may result in the poor representation of cloud cover within 7.5 km of the coast. During pre-operational tests this was not found to be a problem.

4. Results of validation tests

The code for the new IR-based detection scheme was fully tested using both archived and real-time data. Data were archived three times per day (at 0230, 1200 and 1430 UTC on even numbered days and 0430, 1300 and 2000 UTC on odd numbered days) on Nimrod in the periods 22/11/2000 - 31/12/2000 and 01/02/2001 - 31/03/2001. This resulted in 248 cases (121 daytime, 127 night-time). These data were used to check the operation of the code, to determine the most appropriate offset and to verify that the new IR-based cloud detection scheme is an improvement on the old IR-based cloud detection scheme.

The problem in validating the performance of the new IR cloud detection scheme is the lack of a data source that can be used as "the truth". It was decided that the cloud cover analyses could be validated in two ways:

(1) Using daytime cases statistically compare the cloud cover analyses from the IR-based schemes with the cloud cover analysis from the old operational scheme (using the old IR scheme and visible scheme, as described in Section 1.1).
(2) Visual inspection of the cloud cover from the old and new IR-based scheme, the old operational scheme (IR and visible-based components) and Meteosat visible and IR images.

4.1. Statistical performance of the new IR-based cloud detection scheme

		Test scheme (IR thresholding)	
		Cloud	Clear
Old operational daytime scheme (IR & visible thresholding)	Cloud	A	B
	Clear	C	D

Table 3. Confusion table used to compile statistics. Here, the old operational scheme in the daytime (using IR and visible thresholding techniques) is considered to be the best representation of "the truth". The test scheme under consideration may be the old IR-based scheme or the new IR-based scheme with various offsets. The total number of grid points is N (N = A+B+C+D).

Six statistical parameters were used to assess the accuracy of various IR-based cloud detection schemes. The test schemes consisted of the new IR-based scheme with different offsets and the old IR-based scheme. The statistical parameters used are based on a confusion table shown in Table 3. Each grid point in the cloud cover analysis from the test scheme is compared to the equivalent grid point in the cloud cover analysis from the old operational scheme. For example, if a grid point in the test scheme is labelled cloudy but the same grid point in the old operational scheme is labelled clear, then a unit will be added to variable C. The following statistics were computed:

Hit rate:

$$HIT = \frac{A+D}{N}, \quad (4)$$

Probability of detection:

$$POD = \frac{A}{A+B}, \quad (5)$$

False alarm ratio:

$$FAR = \frac{C}{A+C}, \quad (6)$$

Bias:

$$BIAS = \frac{A+C}{A+B}, \quad (7)$$

Heidke skill score:

$$HSS = \frac{2(AD-BC)}{(A+B)(B+D)+(A+C)(C+D)}, \quad (8)$$

Equitable threat score:

$$ETS = \frac{(A-(A+C)(A+B)/N)}{((A+B+C)-(A+C)(A+B)/N)}. \quad (9)$$

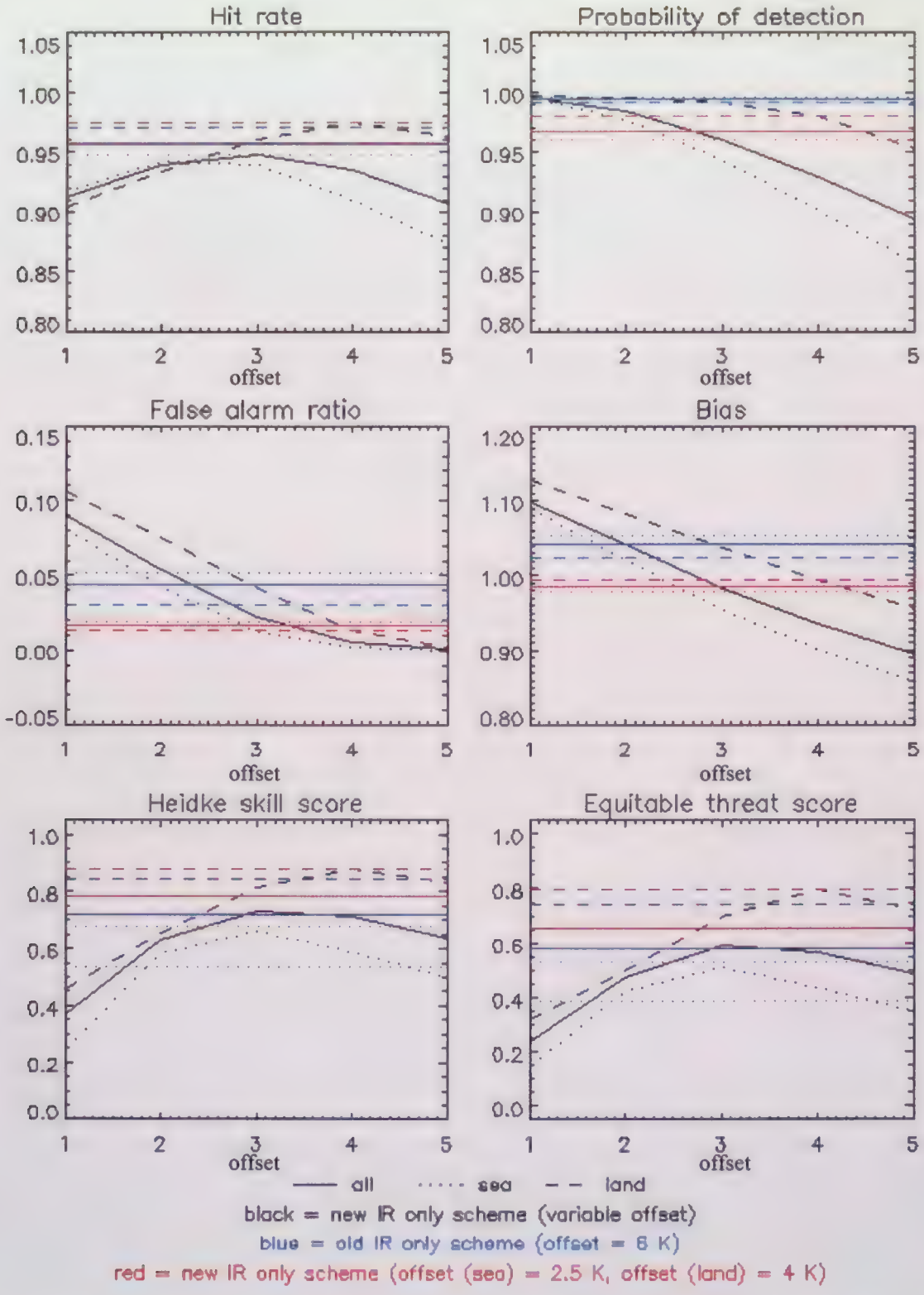

Figure 6. Mean statistics for all the daytime archived data (121 cases). The graphs show the mean statistical value for cloud cover analyses derived using (i) the new IR-based scheme with offsets of between 1 K and 5 K (as indicated by the values along the x-axes) (black lines), (ii) the old IR-based scheme with a fixed offset of 6 K (blue lines) and (iii) the new IR-based scheme with a offset of 2.5 K over the sea and 4 K over the land (red line). In each case the statistics have been calculated for grid points over the sea (dotted lines), over the land (dashed lines) and for all grid points (solid lines).

(a) Mean values for all archived daytime cases (121 cases):

Scheme	Offset (K)	HIT	POD	FAR	BIAS	HSS	ETS
New IR-based scheme	1.0	0.91	**0.99**	0.09	1.10	0.37	0.24
	2.0	0.94	0.98	0.05	1.04	0.63	0.47
	3.0	0.95	0.96	0.02	0.98	0.73	0.59
	4.0	0.93	0.93	0.01	0.94	0.71	0.57
	5.0	0.91	0.89	**<0.01**	0.89	0.64	0.48
	2.0 (sea) & 4.0 (land)	**0.96**	0.98	0.03	**1.01**	0.77	0.63
	2.5 (sea) & 4.0 (land)	**0.96**	0.97	0.02	0.98	**0.79**	**0.66**
	3.0 (sea) & 4.0 (land)	0.95	0.96	0.01	0.97	0.78	0.65
Old IR-based scheme	6.0	**0.96**	**0.99**	0.04	1.04	0.72	0.57

(b) Mean values for all archived daytime cases in November 2000 (14 cases):

Scheme	Offset (K)	HIT	POD	FAR	BIAS	HSS	ETS
New IR-based scheme	1.0	0.92	**1.00**	0.07	1.07	0.29	0.18
	2.0	0.94	0.98	0.04	1.03	0.56	0.40
	3.0	0.95	0.95	0.02	0.97	0.69	0.54
	4.0	0.93	0.92	**<0.01**	0.92	0.66	0.50
	5.0	0.90	0.89	**<0.01**	0.89	0.58	0.41
	2.0 (sea) & 4.0 (land)	**0.96**	0.98	0.02	**1.00**	0.75	0.60
	2.5 (sea) & 4.0 (land)	**0.96**	0.96	0.01	0.98	**0.76**	**0.62**
	3.0 (sea) & 4.0 (land)	0.95	0.95	0.01	0.96	0.74	0.60
Old IR-based scheme	6.0	**0.96**	**1.00**	0.04	1.04	0.63	0.48

(c) Mean values for all archived daytime cases in December 2000 (32 cases):

Scheme	Offset (K)	HIT	POD	FAR	BIAS	HSS	ETS
New IR-based scheme	1.0	0.91	**1.00**	0.09	1.10	0.25	0.15
	2.0	0.93	0.99	0.06	1.06	0.54	0.38
	3.0	0.95	0.97	0.03	**1.00**	0.71	0.56
	4.0	0.94	0.94	0.01	0.95	0.70	0.55
	5.0	0.91	0.90	**<0.01**	0.90	0.63	0.47
	2.0 (sea) & 4.0 (land)	**0.96**	0.98	0.03	1.01	0.74	0.60
	2.5 (sea) & 4.0 (land)	**0.96**	0.97	0.02	0.99	**0.77**	**0.64**
	3.0 (sea) & 4.0 (land)	**0.96**	0.96	0.01	0.98	**0.77**	**0.64**
Old IR-based scheme	6.0	**0.96**	**1.00**	0.04	1.04	0.67	0.53

(d) Mean values for all archived daytime cases in February 2001 (38 cases):

Scheme	Offset (K)	HIT	POD	FAR	BIAS	HSS	ETS
New IR-based scheme	1.0	0.90	**1.00**	0.11	1.13	0.48	0.33
	2.0	0.94	0.98	0.06	1.05	0.71	0.55
	3.0	0.95	0.97	0.03	0.99	0.80	0.67
	4.0	0.94	0.94	0.01	0.95	0.80	0.67
	5.0	0.92	0.90	**<0.01**	0.90	0.73	0.59
	2.0 (sea) & 4.0 (land)	**0.96**	0.98	**<0.01**	**1.01**	0.82	0.70
	2.5 (sea) & 4.0 (land)	**0.96**	0.97	0.02	**0.99**	**0.84**	**0.73**
	3.0 (sea) & 4.0 (land)	**0.96**	0.96	0.01	0.98	**0.84**	0.72
Old IR-based scheme	6.0	**0.96**	0.99	0.04	1.04	0.82	0.69

(e) Mean values for all archived daytime cases in March 2001 (37 cases):

Scheme	Offset (K)	HIT	POD	FAR	BIAS	HSS	ETS
New IR-based scheme	1.0	0.92	**1.00**	0.08	1.08	0.39	0.25
	2.0	0.95	0.98	0.04	1.02	0.66	0.50
	3.0	0.94	0.95	0.01	0.97	0.71	0.56
	4.0	0.92	0.92	**<0.01**	0.92	0.66	0.50
	5.0	0.89	0.88	**<0.01**	0.88	0.57	0.41
	2.0 (sea) & 4.0 (land)	**0.96**	0.97	0.02	**1.00**	0.75	0.60
	2.5 (sea) & 4.0 (land)	0.95	0.96	0.01	0.97	**0.76**	**0.62**
	3.0 (sea) & 4.0 (land)	0.95	0.95	0.01	0.95	0.73	0.59
Old IR-based scheme	6.0	**0.96**	0.99	0.04	1.04	0.70	0.55

Table 4 (previous page). Mean values of six statistical parameters for the new IR-based scheme with various offsets, including three where the offset differs over sea and land, and the old IR-based scheme. Table (a) shows the mean values for all the archived daytime cases. Tables (b) to (e) show the mean values for each month (November, December, February, March for the winter of 2000/01). In each table, the best mean value for each statistical parameter is highlighted in bold script.

In order to determine the optimum offset to use in the new IR-based cloud detection scheme and to show that the new IR-based scheme is an improvement on the old IR-based scheme all six statistical parameters have to be assessed in a balanced way. For example, a high HIT and POD are desirable, but these may result in a high FAR and BIAS (greater than 1.0) and low HSS and ETS and so the scheme with this offset does not produce the best overall cloud cover analysis. Ultimately, an IR-based scheme that achieves high skill scores (HSS and ETS), with fairly high HIT and POD and a low FAR is required. The value of the bias is also important, and in general a scheme with a bias of 1.0 gives the best cloud cover analysis. Figure 6 and Tables 4(a) to 4(e) show the statistical parameters for all the daytime cases in the archived dataset for several IR-based test schemes. The main observations made from these statistics are listed below.

- In general, the highest HIT and POD were obtained under the old IR-based scheme, with mean values over the whole archived dataset of 0.96 and 0.99, respectively. This demonstrates that the old IR-based scheme detects the most cloudy grid points of all the schemes tested. However, the statistics show that the old IR-based scheme overestimates the amount of cloud, with a bias of 1.04 and a FAR of 0.04 indicating that 4% of grid points were labelled cloudy by the old IR-based scheme when the daytime operational scheme had labelled the grid points clear.

- Initially, statistics were computed for the new IR-based scheme with the same offset used over the sea and the land of between 1.0 K and 5.0 K (black lines in Figure 6). The first observation to be made from Figure 6 is that the values of the statistical parameters for sea and land grid points can be quite different. However, of these schemes an offset of 3.0 K applied over both surface types gives the best skill scores (0.73 and 0.56 for the HSS and ETS respectively). The bias is 0.98 (and was 1.00 for December 2000), and the HIT and POD are quite high. However, it was found that the skill scores could be improved by using different offsets over the land and the sea.

- Over the land it is clear that a offset of 4.0 K produces the best statistics for all four months that were studied, as shown by the graphs in Appendix 1. The mean statistical values for the land based grid points using an IR scheme with a 4.0 K offset for all the daytime archived data are:

  HIT = 0.98 FAR = 0.01 HSS = 0.88
  POD = 0.98 BIAS = 0.99 ETS = 0.80

- Initially, the optimum offset for use over the sea was not clear. The series of graphs in Appendix 1 show that in most cases an offset of 3.0 K gives the best statistics overall. However, the mean bias for grid points over the sea in November 2000, December 2000 and March 2001 was closer to 1.0 for a 2.0 K offset. Moreover, the HIT in November 2000 and March 2001 was higher for an IR-based scheme with a 2.0 K offset than for a scheme with a 3.0 K offset over the sea. IR-based detection schemes with an offset of 4.0 K over the land and the following offsets over the sea were tested:

  (i) 3.0 K
  This scheme had a significantly lower FAR than the old IR-based scheme. The reason for this is that this scheme has a low bias of 0.97, underestimating the amount of cloud, thus reducing the number of false alarms. The bias over the sea is low, at only 0.95. The skill scores, HSS and

ETS, are higher than the old IR-based scheme. In general the HIT showed an improvement over the old scheme for the land based grid points (0.01 higher), but it was degraded for grid points over the sea. The mean values for the sea based grid points for all the daytime archived data are:

HIT = 0.94	FAR = 0.01	HSS = 0.68
POD = 0.94	BIAS = 0.95	ETS = 0.53

(ii) 2.0 K

The decrease in the offset over the sea from 3.0 K to 2.0 K resulted in a bias closer to 1.0, thus improving the balance between overestimating and underestimating the number of cloudy grid points. The HIT and POD increased, compared to the scheme with a 3.0 K offset, but the HSS and ETS were degraded. The mean values for the sea based grid points for all the daytime archived data are:

HIT = 0.95	FAR = 0.04	HSS = 0.63
POD = 0.96	BIAS = 1.01	ETS = 0.47

(iii) 2.5 K

This scheme showed an improved bias compared with the scheme with the 3.0 K offset, and only a 0.01 depreciation on the bias of the scheme with a 2.0 K offset. However, the skill scores are identical to those for the scheme with the 3.0 K offset, and much better than those for the old IR-based scheme. For comparison, the old IR-based scheme had skill scores of 0.54 and 0.39 for HSS and ETS respectively for grid points over the sea. The mean values for the sea based grid points for all the daytime archived data are:

HIT = 0.95	FAR = 0.02	HSS = 0.68
POD = 0.96	BIAS = 0.98	ETS = 0.53

- Statistically, the optimum offsets for the new IR-based detection scheme were found to be 4.0 K over the land and 2.5 K over the sea. A scheme with these offsets produces a statistically better representation of the cloud cover than the old IR-based scheme.

The optimum offsets for the new IR-based scheme ultimately depend on the application of the cloud cover analysis. There are, in general, two solutions that may be considered to give the best cloud cover analysis:

(1) Where the cloud detection scheme produces a cloud cover analysis that gives the best representation of the clear and cloudy areas, i.e. with a bias of 1.0. This scheme may misclassify some grid points as clear or cloudy.
(2) Where the cloud detection scheme detects all the cloud. This scheme may overestimate the amount of cloud by misclassifying clear grid points as cloud and it will have a bias of greater than 1.0.

The assumption has been made that it is the best representation of cloud cover that is needed for Nimrod. However, if at a later stage it is decided that it is important to aim to detect all cloud, then the bias of the scheme can be increased by changing the offsets using the results presented here.

4.2. Visual inspection

Several cases are shown in this section that attempt to illustrate the range of situations that have occurred during testing. The descriptions given below refer to the images in the figures in the following pages. In addition to inspecting the cloud cover analyses from the archived data, real-time cloud cover maps were also monitored during the pre-operational tests.

4.2.1. Selection of the optimum offsets: example on 28/02/2001

The selection of appropriate offsets to use in the new IR-based scheme by visual inspection can be demonstrated using the example shown in Figure 7. The Meteosat IR and visible images (Figures 7(a) and 7(b)) show that the area is largely covered in cloud except in areas of convective cloud where there are clear patches, e.g. to the south-west, west and north of Ireland, small areas over the North Sea and over the Norwegian mountains. Figures 7(f) to 7(j) illustrate the effect on the cloud cover analysis of using different offsets with the new IR-based scheme. By comparing these analyses with the cloud cover analysis from the old daytime operational scheme (Figure 7(c)) it can be seen that a new IR-based scheme with an offset of 2.0 K or 3.0 K produces a similar cloud cover analysis. Figure 7(e) shows the cloud cover analysis from the new IR-based scheme with offsets of 2.5 K and 4.0 K over the sea and land respectively. Of all the cloud cover analyses presented in Figure 7, it is Figure 7(e) that most closely resembles the cloud cover analysis produced by the old daytime scheme (Figure 7(c)). This agrees with the results of the statistical studies. An area where they do differ is in the North Sea between Scotland and Norway. Here, the analysis from the old daytime scheme has complete cloud cover, but the analysis from the new IR-based scheme (Figure 7(e)) shows an area of clear sky. Visual inspection of the Meteosat imagery indicates that there is an area of clear sky in this region. Thus, in this case, the new IR-based scheme has produced a better cloud cover analysis than the old daytime scheme (combined IR and visible thresholding).

4.2.2. Sunrise on 16/10/2001

Figure 8 shows a fairly typical example of the performances of the old and new cloud detection schemes at sunrise. Both of the cloud cover analyses presented in Figure 8 were generated using the daytime schemes (i.e. combining estimates from the visible-based and IR-based schemes). At 0700 UTC on 16/10/2001 about 40 % of the visible image contains valid data. The old scheme first estimates the cloud cover using the night-time scheme, i.e. using the old IR-based scheme with an offset of 6.0 K. Where there is valid Meteosat visible data, the cloud cover is computed using the daytime scheme, i.e. using the old IR-based scheme with an offset of 7.5 K and the visible thresholding scheme. The different schemes used in the lit and unlit portions of the Nimrod domain cause a discrepancy in the cloud cover analysis between the two portions. Examination of the Meteosat IR image indicates that a large area over the North Sea is cloud free, but the old scheme analysis shows almost full cloud cover (Figure 8(a)). This demonstrates the reliance of the accuracy of the old scheme on the visible thresholding technique. In contrast, the new scheme appears to provide a good representation of the clear and cloudy areas in the unlit portion of the Nimrod domain (Figure 8(b)). There is continuity in the cloud cover analysis across the edge of the lit portion of the Nimrod domain e.g. from The Netherlands to the North Sea. This shows the smooth transition between night-time and daytime schemes, and demonstrates that the new scheme operates satisfactorily without valid visible data. Situations such as the one presented in Figure 8 occurred regularly during pre-operational tests.

4.2.3. Comparison with NNCC at sunrise on 02/10/2001

The Neural Network Cloud Classifier (NNCC) uses Meteosat IR and visible imagery to estimate the cloud type (Pankiewiez et al., 2000). It is interesting to compare the NNCC output with the cloud cover analyses from the old and new cloud detection schemes because the NNCC does not use MES data and uses a very different method to generate a cloud cover map. The NNCC output, the cloud cover analyses (from old and new schemes), and Meteosat imagery have been monitored for over a month using real-time data in pre-operational testing. In general, the NNCC output and the cloud cover analysis from the new scheme (IR and visible thresholding) were in good agreement in the amount and distribution of cloud. However, it was noted that the new cloud detection scheme showed an improvement over the NNCC in the detection of low level dynamic cloud.

Figure 9 shows an example of the cloud cover analyses, the NNCC output and Meteosat imagery on 04/10/2001 at 0730 UTC. There are significant differences between the cloud cover analyses from the new and old schemes (Figures 9(c) and 9(d)). These are mostly over the sea, e.g. north-western area of Nimrod domain and over the North Sea. In these areas the cloud cover analysis from the new scheme shows clear patches whilst the cloud cover analysis from the old scheme shows cloud. The output from the NNCC fairly closely matches the cloud cover analysis from the new scheme in these areas. Visual inspection of the Meteosat imagery indicates that there are clear areas over the north-western region of the Nimrod domain and the North Sea. Over the land, the cloud cover from the old scheme is quite accurate.

There are some differences between the NNCC output and the cloud cover analysis from the new scheme, which are due in part to the larger pixels used in the NNCC. One area where they differ is over East Anglia and southern area of the North Sea. Here, the NNCC shows a clear region, whilst the cloud cover analysis from the new scheme has some small clear patches amongst cloud. It is difficult to determine which of these two analyses is the most accurate from inspection of the Meteosat imagery. The IR image shows warm BTs in this region. However, the visible image does show some variation in reflectance over the region which may indicate the presence of low level cloud.

4.2.4. Underestimation of cloud cover on 09/03/2001

There are two situations that have been noted in which the new IR-based cloud detection scheme can perform poorly. These are the detection of low level cloud at high latitudes and the detection of fog. The example presented in Figure 10 shows the poor performance of the new IR-based scheme in both of these situations.

The Meteosat images show an area of warm convection in the north-west of the Nimrod domain. The shallow convective cloud can clearly be seen in the Meteosat visible image, but not in the IR image due to its warm temperature. The cloud cover analysis from the new IR-based scheme (Figure 10(c)) shows a clear area to the north-west of Scotland in this region of shallow convective cloud. However, the cloud cover analysis from the old IR-based scheme (Figure 10(d)) shows complete cloud cover. Neither of these analyses is very accurate, since there are both cloudy and clear patches in this region. The old IR-based scheme tends to overestimate the cloud cover, particularly over the sea at high latitudes. This is in part due to the fact that a constant offset is used over the whole of the Nimrod domain, regardless of the magnitude of the Meteosat zenith angle. As the zenith angle increases so the atmospheric deficit (discussed in Section 3.2.3.) tends to increase; this is not accounted for in the old IR scheme. However, the new IR scheme does account for this effect via the RTTOV simulations. A possible explanation for the poor performance of the new IR scheme in the case presented in Figure 10 is that the simulated clear sky BT calculations in this

region are too low. This may be because the simulation of the atmospheric absorption along the satellite viewing path is too strong or the decrease in emissivity with satellite zenith angle is too great, so that at large zenith angles the simulated BT is too low. Other explanations may be that the MES forecast temperature and humidity profiles are incorrect or that the offset is too large.

The Meteosat images in Figure 10 show an area of low level cloud, probably fog, off the coast of The Netherlands and Germany. Neither the new or the old IR-based schemes detected this area of fog, although it was detected by the visible based scheme. This is a problem that is not easily solved for the new IR-based detection scheme. Even if the offset over the sea were reduced to 1.0 K only a small area of the fog would be detected (image not shown). In this situation greater spectral information is required to differentiate between warm fog and clear sea. The information that will be available from the SEVIRI instrument on MSG should allow more accurate cloud cover analyses in these situations.

It should be stressed that in all the archived daytime cases examined (121 cases) there were only a few cases (approximately 4) that were noted to underestimate the cloud cover at high latitudes and only a couple of cases in which the new IR scheme performed poorly in areas of fog. Therefore, compared to the large improvements made to the cloud cover analysis by the introduction of the new IR-based scheme, these problems are relatively minor.

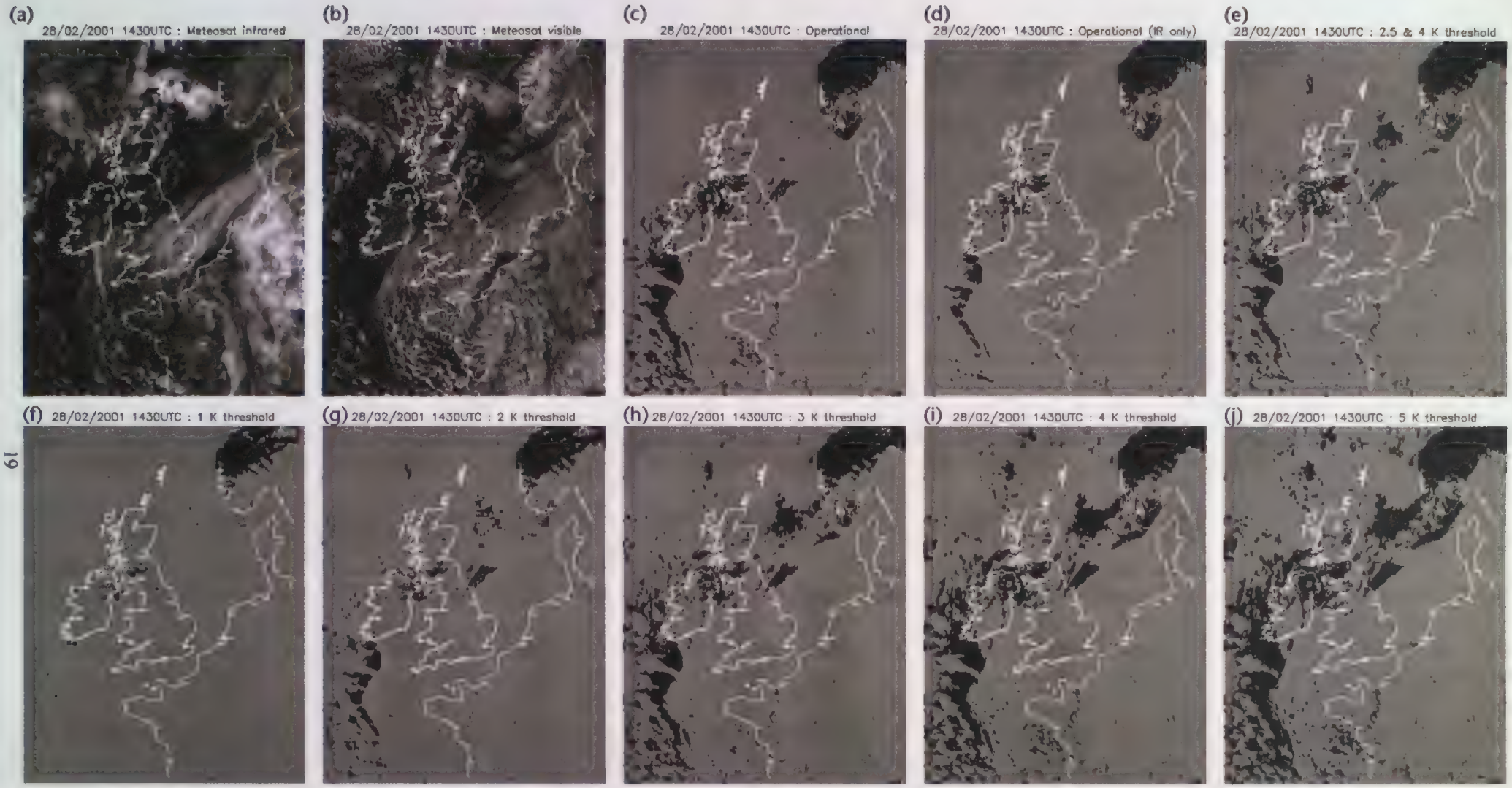

Figure 7. Meteosat imagery and cloud cover analyses on 28/02/2001 at 1430 UTC. (a) and (b) are Meteosat IR and visible images for 1430 UTC. MES forecast fields valid at 1400 UTC were used to generate the cloud cover analyses, (c) to (j). Cloud cover analysis (c) is from the old operational daytime scheme, whilst (d) is from the old IR-based scheme and (e) is from the new IR-based scheme (with an offset of 2.5 K over the sea and 4.0 K over the land). Cloud cover analyses (f) to (j) are from the new IR-based scheme with offsets varying from 1.0 K to 5.0 K.

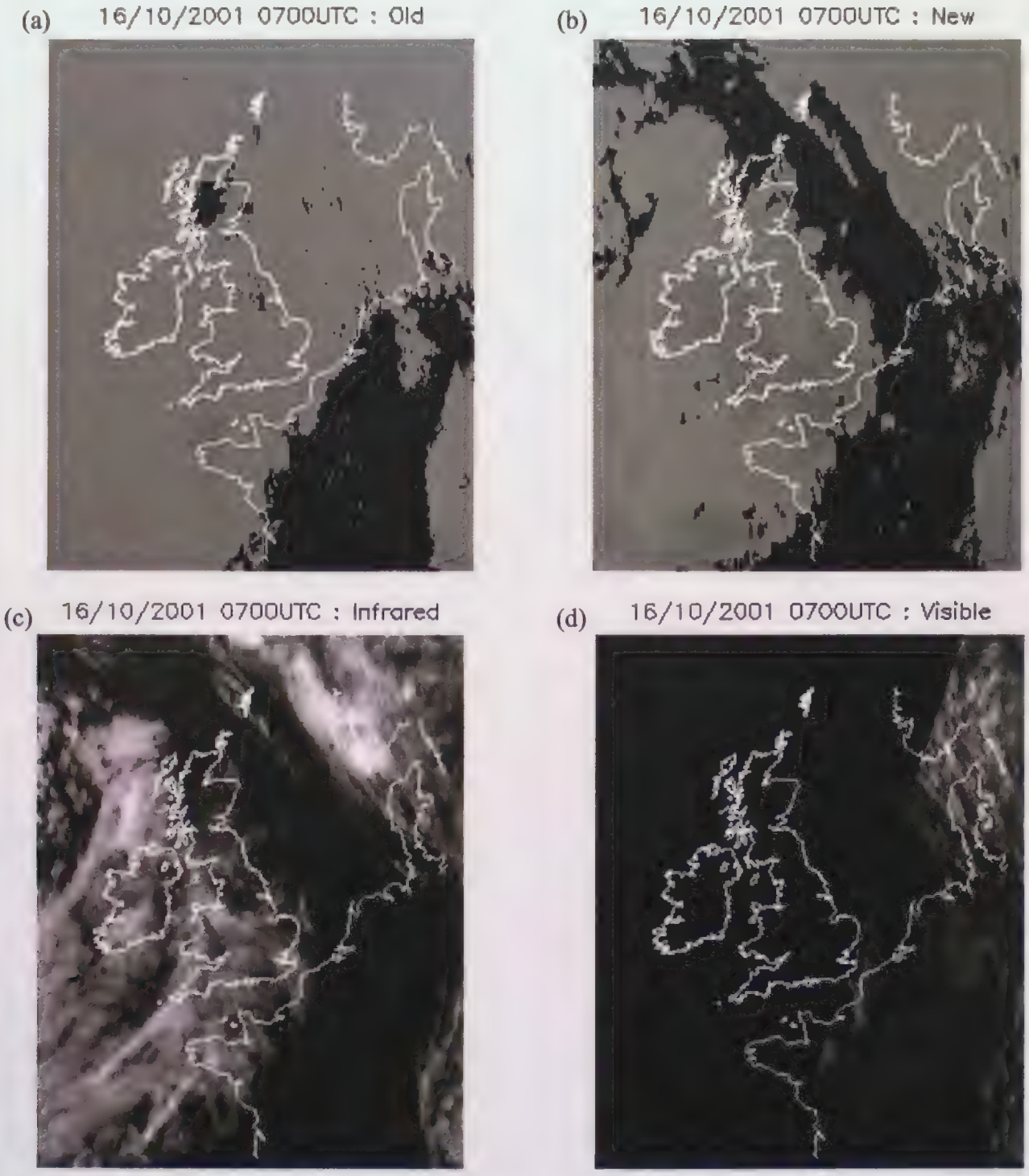

Figure 8. Cloud cover analyses generated by (a) the old cloud detection scheme and (b) the new cloud detection scheme (both using infrared and visible imagery where available) and Meteosat (c) IR and (d) visible imagery at 0700 UTC on 16/10/01. In the cloud cover analyses, clear areas are black and cloudy are grey.

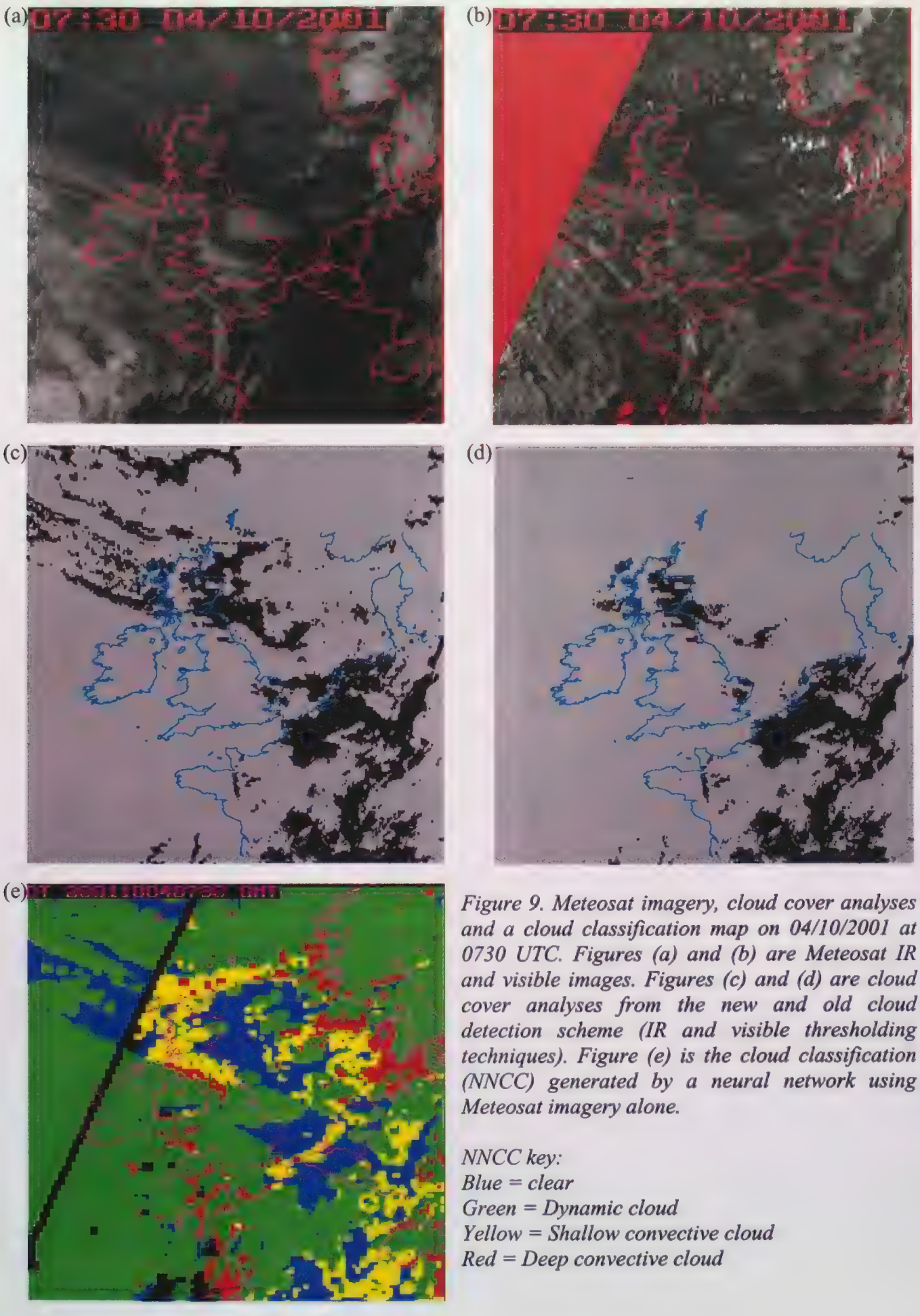

Figure 9. Meteosat imagery, cloud cover analyses and a cloud classification map on 04/10/2001 at 0730 UTC. Figures (a) and (b) are Meteosat IR and visible images. Figures (c) and (d) are cloud cover analyses from the new and old cloud detection scheme (IR and visible thresholding techniques). Figure (e) is the cloud classification (NNCC) generated by a neural network using Meteosat imagery alone.

NNCC key:
Blue = clear
Green = Dynamic cloud
Yellow = Shallow convective cloud
Red = Deep convective cloud

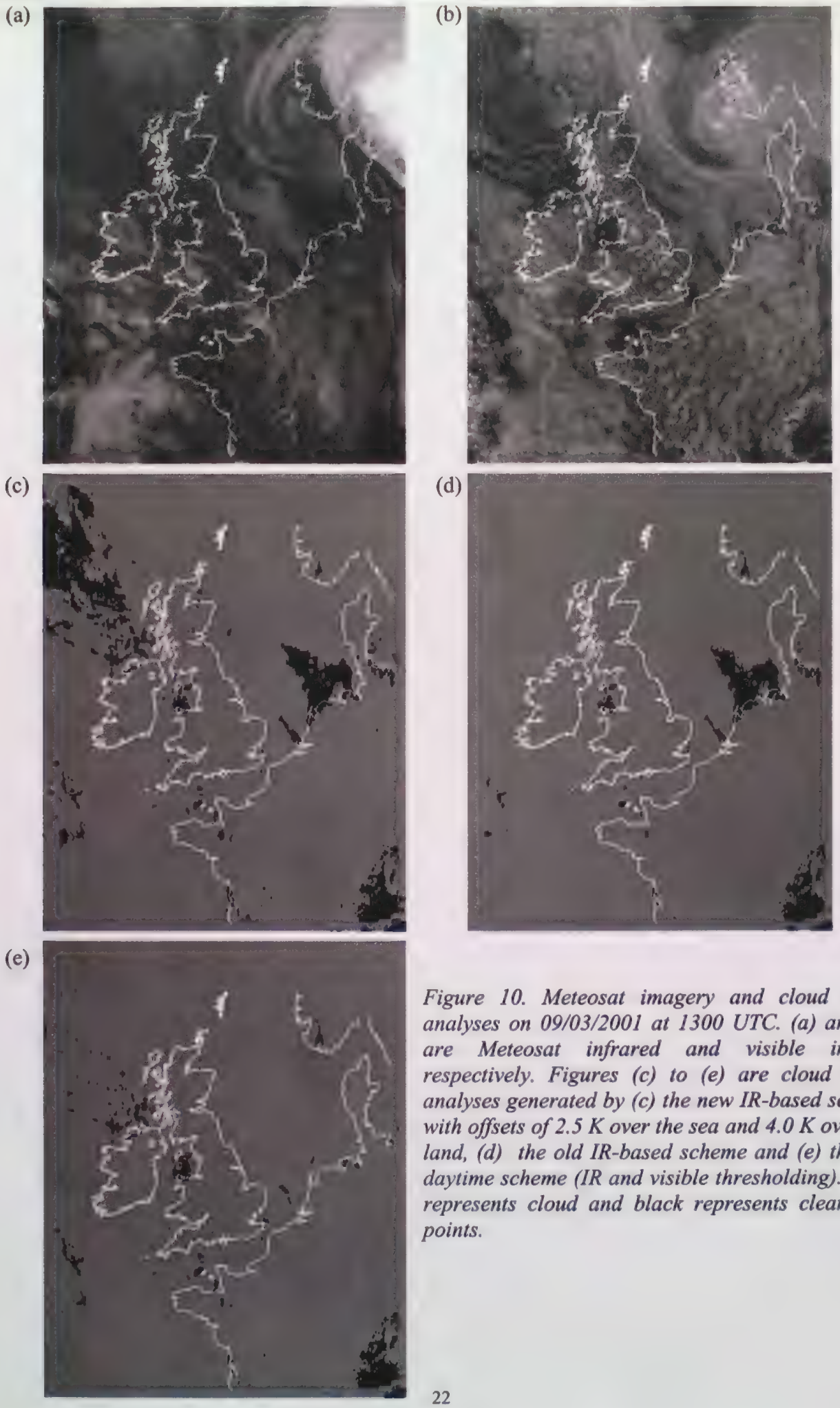

Figure 10. Meteosat imagery and cloud cover analyses on 09/03/2001 at 1300 UTC. (a) and (b) are Meteosat infrared and visible images respectively. Figures (c) to (e) are cloud cover analyses generated by (c) the new IR-based scheme with offsets of 2.5 K over the sea and 4.0 K over the land, (d) the old IR-based scheme and (e) the old daytime scheme (IR and visible thresholding). Grey represents cloud and black represents clear grid points.

5. Description of the code

The code for the cloud detection scheme on Nimrod has been written following the Nimrod Programming Standards, Version 2.05 (Harrison, 1994). Fortran 90 has been used except where it conflicts with the Nimrod Programming Standards. The code has been reviewed by a member of the Nimrod team and has been fully tested for over a month on NIMR2, a mirror machine to Nimrod, to check for bugs and ensure that the code is robust.

5.1. Code structure and sequence of events

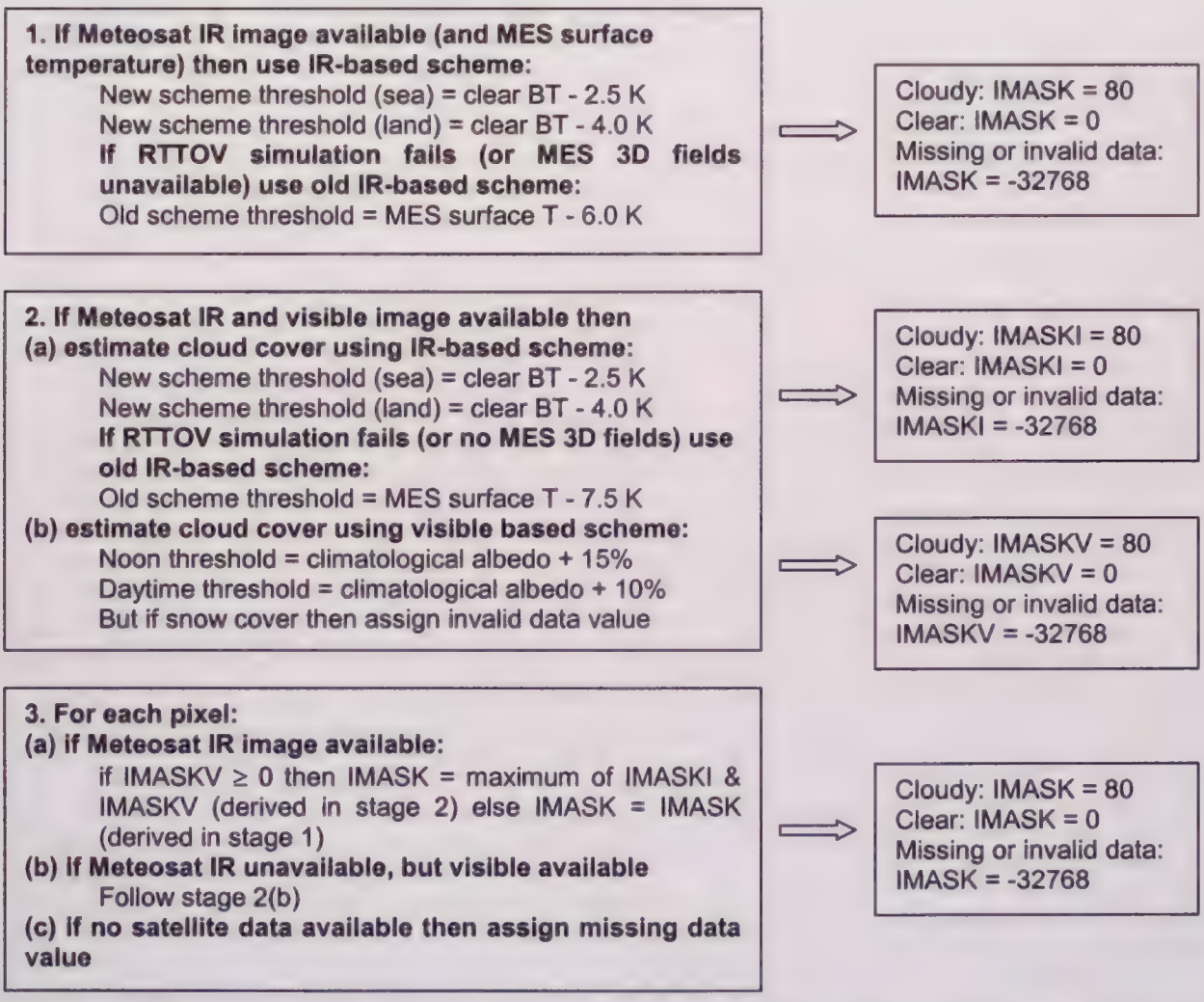

Figure 11. Schematic of the logic involved in deriving the cloud cover analysis. The cloud cover arrays (IMASK, IMASKI and IMASKV) contain values to represent clear (0), cloudy (80) and missing or invalid data (-32768). Only IMASK is output as a standard Nimrod format file.

Figure 11 illustrates the logic involved in deriving the cloud cover analysis in different circumstances, e.g. at night, when there is snow cover, or missing MES data. The cloud cover analysis is initially derived using the IR-based cloud detection scheme. If Meteosat visible data are unavailable then the IR-based cloud cover is the final output, e.g. at night. If Meteosat visible data are available then the cloud cover is estimated using the IR-based scheme (array IMASKI) and the visible based scheme (array IMASKV). These are combined to produce the final output cloud cover array (IMASK).

The structure of the cloud detection code is shown graphically in Appendix 2. It largely follows the same structure as the old cloud detection scheme, but with some subroutines replaced and others added. A major difference is that the cloud detection part of the satellite processing script now consists of two parts:

(i) Calculation of the clear sky brightness temperature for each grid point in the 15 km Nimrod grid using MES forecast fields and RTTOV code (see Section 3). This is performed every hour, at approximately 2.5 minutes past the hour.

(ii) Estimation of the cloud cover on a 5 km grid. This is performed every 30 minutes, at 2.5 minutes past the hour (after the RTTOV simulations) and at 32.5 minutes past the hour. These both use the simulated clear sky BT valid for the hour (00 minutes).

Time (UTC)	Event
1200 (nominal time)	MES run
1500 +	1200 UTC MES run forecast data received on Nimrod
1600	(i) RTTOV simulation using 1200 UTC forecast fields valid for 1600 UTC (ii) Cloud cover determined using output from (i) and 1600 UTC Meteosat IR image
1630	Cloud cover determined using output from (i) valid at 1600 UTC and 1630 UTC Meteosat IR image
1800	MES run

Table 5. Sequence of events leading to the generation of cloud cover maps at 1600 UTC and 1630 UTC using the new cloud detection scheme. The time between the run time of the MES and the availability of the forecast data on Nimrod is variable, but it is approximately 3-4 hours.

Table 5 shows the sequence of events that lead to the generation of a cloud cover analysis. In the example shown in Table 5 the forecast lead time is only 240 minutes, but lead times may be up to 540 minutes, or greater if a MES run fails. For example, the 1500 UTC cloud cover analysis would be generated using MES forecast data from the 0600 UTC run with a lead time of 540 minutes.

5.2. Run time and flexibility

The length of time for code to run on Nimrod is critical. Currently, there are only 3 minutes between the reception of satellite data on Nimrod and when all satellite based Nimrod products have to be sent to customers. Therefore, careful consideration was given to the optimisation of the code. The average run time on NIMR2 was found to be approximately 12 seconds (calculated from ten runs). Of this, 11 seconds are taken up with the simulation of clear sky BT and only 1 second to perform the thresholding tests. These times are well within the acceptable time limits for the cloud detection scheme.

The code has been written so that any variables that may need to be changed are set in a script. This then executes the program. These are variables such as the run frequency, directory names and the offsets for the IR cloud detection scheme for use over the sea and the land. These offsets can be adjusted as necessary to alter the bias of the cloud detection scheme without the need to recompile the code.

6. Summary

An improved cloud detection scheme has successfully been developed for the Nimrod system. This uses Meteosat IR and visible imagery. The visible-based cloud detection scheme has remained unchanged, whilst the IR-based cloud detection scheme has been significantly improved. The new IR-based scheme uses simulated clear sky BT from RTTOV to generate variable thresholds for each grid point in the Nimrod domain. MES forecast fields are used as inputs to RTTOV along with surface type information and Meteosat zenith angle. The Meteosat IR BT are compared with the simulated clear sky BT to determine whether a pixel is mainly clear or mainly cloudy. At night, only the IR-based cloud detection scheme is used. In the daytime both the IR-based and visible based schemes are used and if either scheme detects cloud, the grid point is labelled cloudy.

Following validation tests involving statistical comparisons and visual inspections of the cloud cover analyses from the new IR-based scheme, the old IR-based scheme and the old daytime (IR and visible) scheme, the following thresholding tests were found to be optimum in the new IR-based scheme:

Over sea: if Meteosat IR BT < clear sky BT - 2.5 K then pixel is cloudy, else pixel is clear
Over land: if Meteosat IR BT < clear sky BT - 4.0 K then pixel is cloudy, else pixel is clear.

The new IR-based cloud detection scheme has a Heidke skill score of 0.79 and an equitable threat score of 0.66, based on 121 daytime cases and using the old operational scheme (IR and visible-based schemes) as "the truth". For comparison, the old IR-based scheme had a Heidke skill score of 0.72 and an equitable threat score of 0.57 for the same cases. A major problem in the old IR-based scheme was the overestimation of cloud over the sea. The new IR-based scheme significantly reduces this bias from 1.05, in the old IR-based scheme, to 0.98. The improvement in the cloud cover analysis is particularly noticeable at sunrise and sunset when there is only valid Meteosat visible image data over part of the Nimrod domain. It is at night and at twilight, especially over the sea, when the greatest gain will be made from the implementation of the new IR-based scheme.

The only problems noted with the new IR-based cloud detection scheme are the underestimation of low cloud at high Meteosat zenith angles and the failure to detect fog in some situations. The former problem may be due to errors in the RTTOV simulation of clear sky BT at high zenith angles, or it could be due to errors in the MES forecast fields. This is an area that could be investigated if it proves to be a persistent problem. Another area that could be investigated is the use of different offsets with the season or time of day (i.e. night or day). During pre-operational tests it was found that the use of constant offsets day and night improved the continuity in the cloud cover analyses at sunrise and sunset, but full validation tests on the use of different offsets in different seasons or times of day were not carried out.

Future work in this area will concentrate on the development of cloud products using SEVIRI data from MSG. It is planned that these will supersede Meteosat based products. If the need arises, it should be possible to adapt the new IR-based cloud detection scheme for use with SEVIRI IR data rather than Meteosat IR data. However, the greater number of channels on SEVIRI offers the opportunity for a superior cloud detection scheme that should not only be more accurate but will also provide more information, such as the specification of whether a pixel is completely cloud filled or only partially cloud filled.

References

Eyre, J.R., (1991). A radiative transfer model for satellite sounding systems. *ECMWF Research Department, Technical Memorandum No. 176, ECMWF, Reading.*

Golding, B., (1998). Nimrod: A system for generating automated very short range forecasts. *Meteorological Applications*, **5**, 1-16.

Harrison, D., (1994). Nimrod Programming Standards (Version 2.05). *Nimrod System Documentation Paper No.1, Internal Report, Met Office, Bracknell.*

Jackson, P., (1995). Thresholding methods for the identification of cloud in Meteosat imagery. *Forecast Research Division, Technical Report No. 154, Met Office, Bracknell.*

Merchant, C.J., Harris, A.J., Murray, M.J. and Zavody, A.M., (1999). Toward the elimination of bias in satellite retrievals of sea surface temperature: 1. Theory, modeling and interalgorithm comparison. *Journal of Geophysical Research*, **104**, 23565-23578.

Pankiewicz, G., Pierce, C. and Watkin, S., (2000). Operational use of a neural network cloud classifier for flood forecasting at the UK Met. Office. *Proceedings of 10th Conference on Satellite Meteorology and Oceanography, American Meteorological Society.*

Saunders, R.W., (2000). RTTOV-6 - Science and Validation Report. *NWP SAF report, URL: www.met-office.gov.uk/sec5/NWP/NWPSAF/rtm/.*

Sherlock, V., (1999). ISEM-6: Infrared Surface Emissivity Model for RTTOV-6. *Forecasting Research Technical Report No.299, Met Office, Bracknell.*

Whyte, K.W., (1998). Experiments with a radiative transfer method for the Nimrod analysis of cloud cover at night using Meteosat imagery. *Internal Report, Met Office, Bracknell*

Acronyms

AVHRR	Advanced Very High Resolution Radiometer
BT	Brightness temperature
ETS	Equitable threat score
EUMETSAT	European organisation for the exploitation of meteorological satellites
FAR	False alarm ratio
HIT	Hit rate
HSS	Heidke Skill Score
IR	Infrared
ISEM-6	Infrared Surface Emissivity Model for RTTOV -6
MES	Mesoscale Model
MSG	Meteosat Second Generation
NNCC	Neural Network Cloud Classifier
POD	Probability of detection
RTM	Radiative Transfer Model
RTTOV	Radiative Transfer model for TOVS
SEVIRI	Spinning Enhanced Visible and Infrared Imager
UTC	Universal time (co-ordinated)

Acknowledgements

I would like to thank Bryan Conway and Rod Brown for their guidance throughout the course of this project. Also, thank you to Stephen Higginson, Stephen Moseley, Richard Standing and Andrew Smith for their respective contributions in collecting data, setting up real-time monitoring, advice about writing code for Nimrod and assistance with the optimisation of the code.

Appendix 1. Graphs of the mean values of the statistical parameters for each month

(i) November 2000

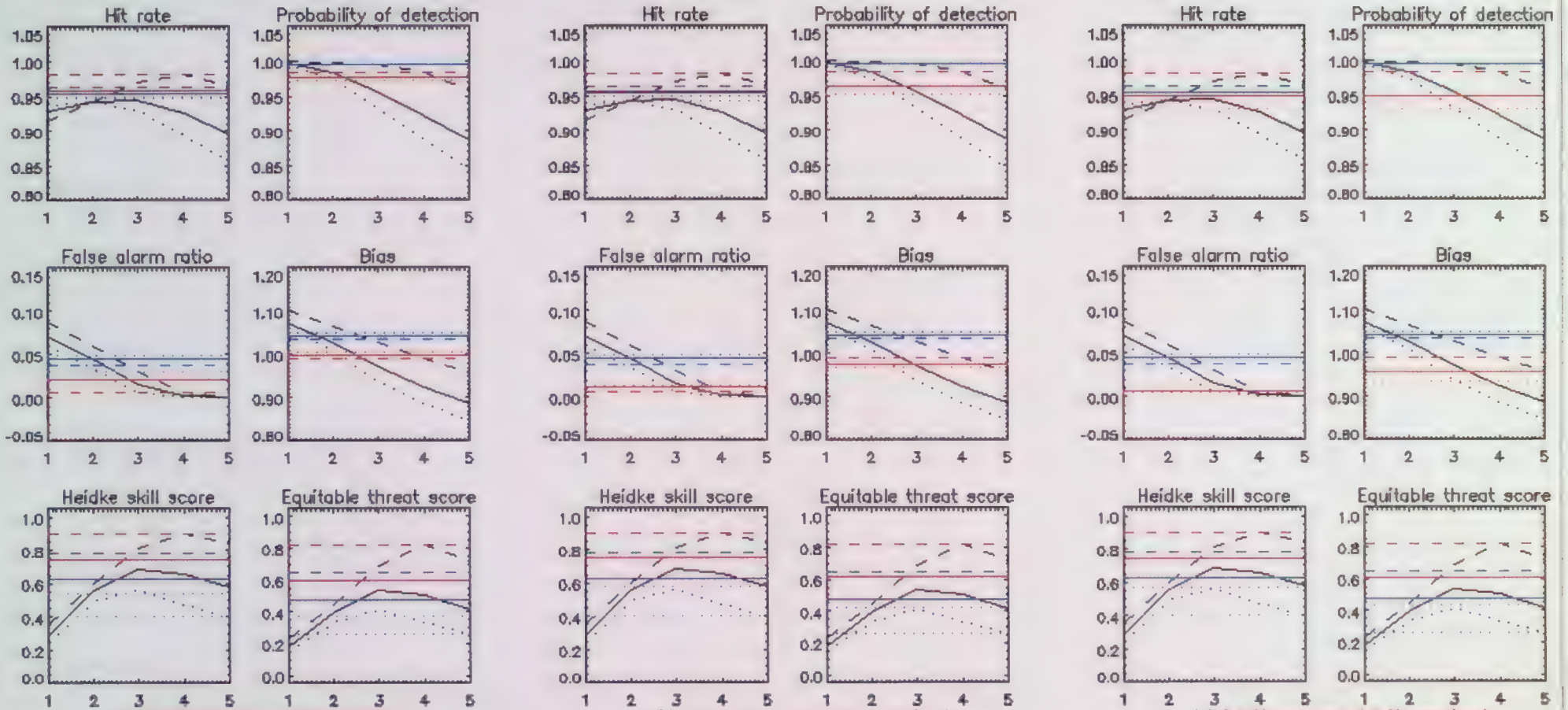

Mean statistical values for 14 daytime cases in November 2000. In each case the statistics have been calculated for grid points over the sea (dotted lines), over the land (dashed lines) and for all grid points (solid lines). All graphs show the mean statistical value for cloud cover maps derived using (i) the new IR-based scheme with thresholds of between 1 K and 5 K (as indicated by the values along the x-axes) (black lines), (ii) the old IR-based scheme with a fixed threshold of 6 K (blue lines) and (iii) the new IR-based scheme with a threshold of(a) 2.0 K over the sea and 4 K over the land, (b) 2.5 K over the sea and 4 K over the land, (c) 3.0 K over the sea and 4 K over the land (red lines).

(ii) December 2000

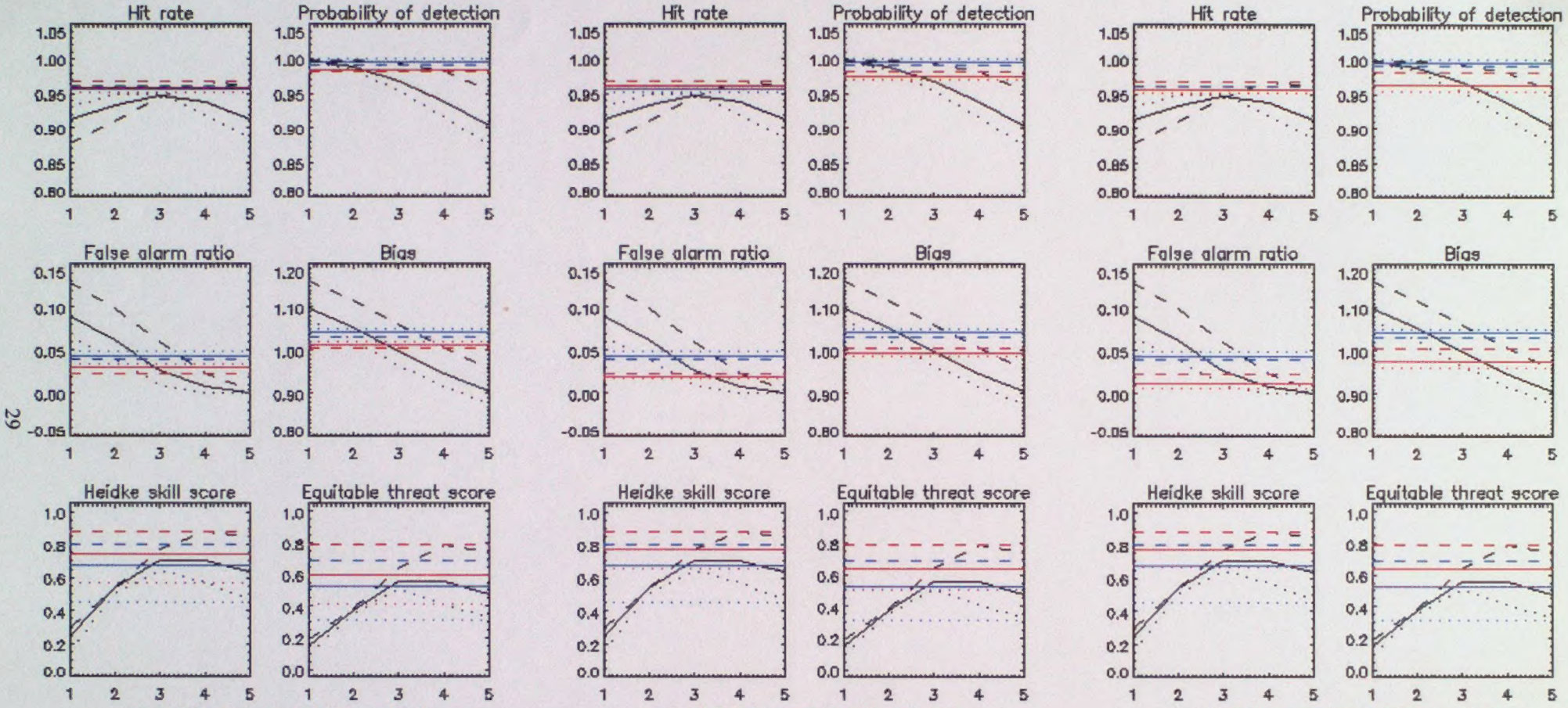

(a) 2.0 K over sea, 4.0 K over land (b) 2.5 K over sea, 4.0 K over land (c) 3.0 K over sea, 4.0 K over land

Mean statistical values for Mean statistical values for 32 daytime cases in December 2000. Annotation is the same as for the graphs in Appendix 1(i).

(iii) February 2001

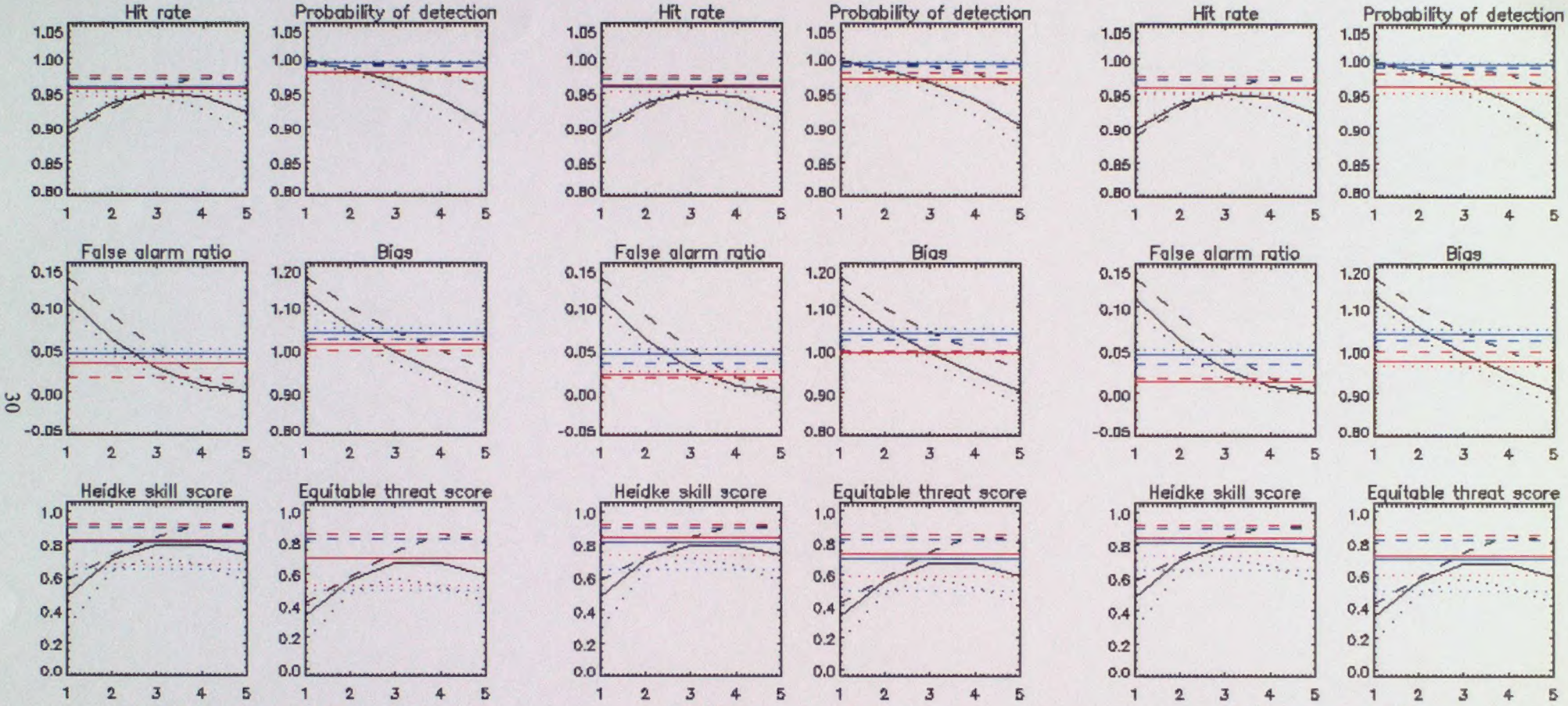

(a) 2.0 K over sea, 4.0 K over land (b) 2.5 K over sea, 4.0 K over land (c) 3.0 K over sea, 4.0 K over land

Mean statistical values for 38 daytime cases in February 2001. Annotation is the same as for the graphs in Appendix 1(i).

(iv) March 2001

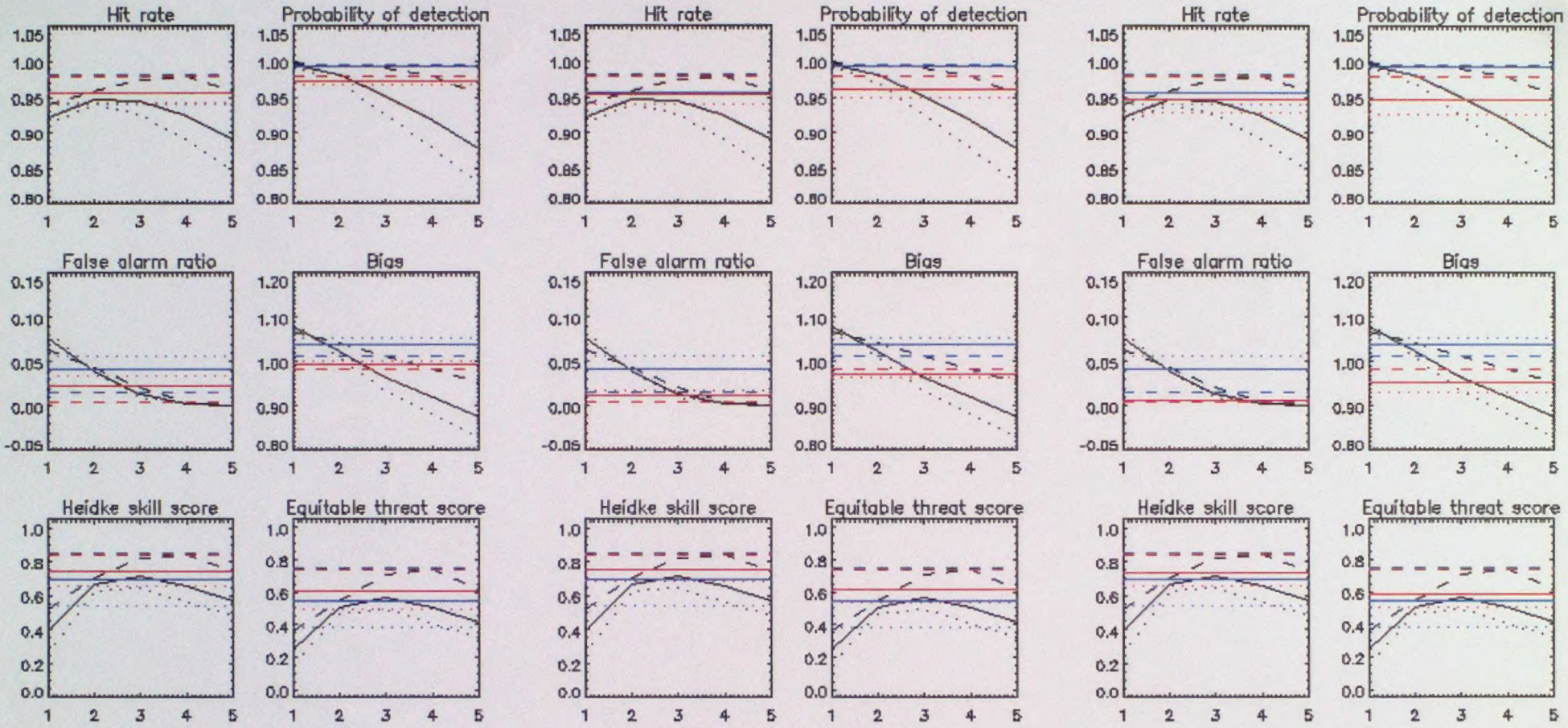

(a) 2.0 K over sea, 4.0 K over land (b) 2.5 K over sea, 4.0 K over land (c) 3.0 K over sea, 4.0 K over land

Mean statistical values for 37 daytime cases in March 2001. Annotation is the same as for the graphs in Appendix 1(i).
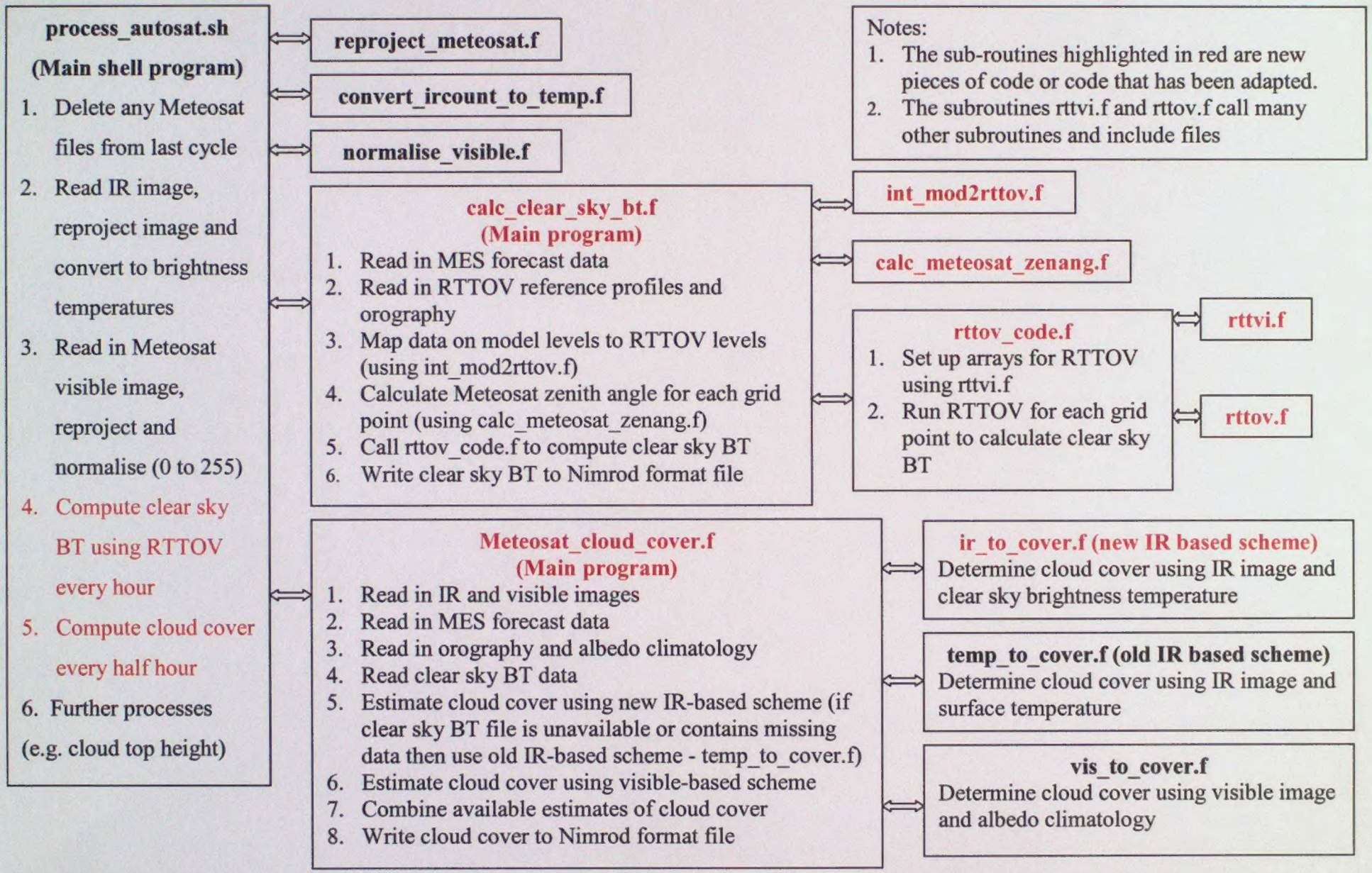
Appendix 2. Structure of the operational cloud detection code on Nimrod